All Conjugate Times of the Rotating Geodesics in the Sub-Riemannian Problem on SE(2)

Igor Moiseev*

October 2026

Abstract

In the standard left-invariant sub-Riemannian problem on the group of plane motions only the rotating geodesics carry conjugate points. Existing results give phase-uniform bounds for the first conjugate time and identify the phases attaining its lower bound. We determine all conjugate times. In the phase–time strip the zero set of Sachkov's reduced Jacobian is, on each of two explicit brackets per Maxwell cell, a closed curve whose two branches have slopes at least one and at most minus one, while a geodesic is a line of slope one; so each geodesic meets it exactly once per bracket. The slope bound is one Riccati identity and the arithmetic–geometric mean inequality. Hence, for every modulus and every initial phase, the first conjugate time is the unique root in Sachkov's bracket. Every Maxwell cell $[p_n^1, p_{n+1}^1)$, $n \geq 1$, carries one root on each of two explicit brackets: two distinct conjugate times except at the critical modulus and one phase, where there is a single conjugate time. For every phase $\psi \not\equiv K$, taken in $(-K, K)$, they obey at large index $p_{(j)} = (j + \frac{1}{2})K - \frac{1}{2}\psi + O(1/j)$: the Jacobian is an exact quadratic in the number of pendulum periods whose leading coefficient is the angular velocity of the geodesic times the Jacobian of the period map.

Keywords: sub-Riemannian geometry, group of motions of the plane, conjugate points, Jacobi elliptic functions, Maxwell strata.
MSC 2020: 53C17, 49K15, 58E10, 33E05.

1 Introduction

Consider the standard left-invariant sub-Riemannian structure on the group of plane motions, in coordinates (x, y, θ),

$$\dot{x} = u_1 \cos\theta, \qquad \dot{y} = u_1 \sin\theta, \qquad \dot{\theta} = u_2, \qquad \int \sqrt{u_1^2 + u_2^2}\, dt \to \min. \tag{1}$$

The normal Hamiltonian system of the maximum principle reduces to the mathematical pendulum, which makes the geodesics explicit in Jacobi elliptic functions [2, 7]. The cut time was identified by Sachkov [10] and the cut locus and optimal synthesis were completed in [11]. Sachkov also proved that only the rotating geodesics carry conjugate points [10, Theorems 2.1, 2.4] and that no conjugate time precedes the cut time [10, Theorems 2.2, 2.3], and stated that the first conjugate time lies in a phase-uniform bracket [10, eq. (2.18)]; the 2023 survey records the result in that bounded form [12, Theorem 2.9].

This paper determines every conjugate time of every rotating geodesic. In Sachkov's rotating coordinates, with $p = t/(2k)$ the time scaled so that the pendulum period is $2K$

*moiseev.igor@gmail.com

and ψ the initial phase, the conjugate equation is $J_2 = 0$ for an explicit reduced Jacobian $J_2 = \alpha \operatorname{sn}^2 \tau + \beta \operatorname{cn}^2 \tau$, $\tau = \psi + p$. Three facts make it solvable.

1. **One ratio.** The coefficients collapse to a single ratio $r(p)$: $J_2 = 0$ if and only if $\operatorname{sn}^2 \tau = r(p)$ ((11), by Lemma 3.1(i)). On each of two brackets per Maxwell cell, $0 < r < 1$, and the zero set in the (p, τ) strip is a closed curve, $\tau = \pm u(p)$ with $u = F(\arcsin \sqrt{r})$ the phase lift of r.
2. **One inequality.** A Riccati identity and the arithmetic–geometric mean inequality give $|u'| \geq 1$ (Lemma 3.2): the two branches of the curve have slopes ≥ 1 and ≤ -1, while a geodesic is the line $\tau = \psi + p$ of slope one.
3. **One crossing.** A line of slope one meets such a curve exactly once (Lemma 3.3): the curve is a one-cover of the phase circle.

The consequences are Theorem 3.4 (the first conjugate time is the unique root in Sachkov's bracket, for every phase, with its extrema), Theorem 4.1 (one root per bracket in every cell $n \geq 1$, with two distinct times except at the critical coalescence) and Theorem 5.1 (the Jacobian is an exact quadratic in the number of pendulum periods, whence the large-index law $p_{(j)} = (j + \frac{1}{2})K - \frac{1}{2}\psi + O(1/j)$ for $\psi \not\equiv K$). The parametrization and Maxwell roots come from [7]; the reduced Jacobian, the sharp phase-uniform bracket and its switch at k_0 are from [10, eqs. (2.10)–(2.19)]. The phase attaining the lower bound, including its uniqueness modulo $2K$, is already characterized in [10, Proposition 2.2].

The central contribution here is the proof of exactly one root on each explicit bracket, including all endpoint phases and the critical coalescence, and hence the complete cell-by-cell count. The proof uses a scalar quotient reduction, the derivative of $\alpha_1 / \operatorname{dn}$, a Riccati product identity and a crossing argument. We also derive the large-index phase law and its locally uniform error estimates, scalar contact and coalescence expansions, an exact count of interior tangencies, eventual folds, and separatrix limits. These derivations supplement the known bounds; the cut time, optimal synthesis, lower-bound phase characterization and standard elliptic identities are reproduced or imported results. The appendices record the concrete Lean construction, coordinate endpoint checks and the scope of the classical variational input. Riccati equations already underlie general conjugate-point comparison theorems [3]; here a scalar factorization specific to the rotating SE(2) Jacobian gives the exact bracket count.

The answer is implicit: for a given phase one inverts a monotone elliptic branch. It is exact, gives a reliable root solver, and yields the phase extrema at once. The conjugate locus as a surface and the inverse problem of counting the geodesics through a point are treated in the companion papers [4, 6], which use the identities of Section 3.

2 Setting

Let $0 < k < 1$ be the elliptic modulus, $k' = \sqrt{1 - k^2}$, $K = K(k)$, $E = E(k)$ the complete integrals, all Jacobi functions of modulus k, and $\mathcal{E}(p) = E(\operatorname{am}(p, k), k) = \int_0^p \operatorname{dn}^2(s, k)\, ds$ Jacobi's epsilon function ($E(\cdot, k)$ the incomplete integral) [8, §22.16(ii)]. We use $\operatorname{sn}' = \operatorname{cn} \operatorname{dn}$, $\operatorname{cn}' = -\operatorname{sn} \operatorname{dn}$, $\operatorname{dn}' = -k^2 \operatorname{sn} \operatorname{cn}$, $\mathcal{E}' = \operatorname{dn}^2$ [8, §22.13(i), §22.16(ii)], the quasi-periodicity $\operatorname{sn}(2nK + s) = (-1)^n \operatorname{sn} s$, $\operatorname{cn}(2nK + s) = (-1)^n \operatorname{cn} s$, $\operatorname{dn}(2nK + s) = \operatorname{dn} s$, the quarter-period shift $\operatorname{sn}(K - s) = \operatorname{cn} s / \operatorname{dn} s$ [8, §22.4], $\mathcal{E}(2nK + s) = 2nE + \mathcal{E}(s)$ [8, §22.16(ii)], and the addition formula

$$\operatorname{sn}^2 x - \operatorname{sn}^2 y = \operatorname{sn}(x + y)\, \operatorname{sn}(x - y) \left(1 - k^2 \operatorname{sn}^2 x\, \operatorname{sn}^2 y\right) \tag{2}$$

(a consequence of the addition theorem [8, §22.8]). In Sections 2–4, s, c, d, ϵ abbreviate $\operatorname{sn} p, \operatorname{cn} p, \operatorname{dn} p, \mathcal{E}(p)$; in Section 5, s is the offset $p - 2nK$.

Rotating geodesics. The normal Hamiltonian system is the pendulum $\dot\gamma = w$, $\dot w = -\sin\gamma$ (w is Sachkov's c) together with $\dot x = \sin\frac{\gamma}{2}\cos\theta$, $\dot y = \sin\frac{\gamma}{2}\sin\theta$, $\dot\theta = -\cos\frac{\gamma}{2}$ [10, eqs. (1.6)–(1.9)]. The rotating stratum is $C_2 = \{H > 1\}$, $H = w^2/2 - \cos\gamma$ the pendulum energy; there the elliptic coordinates are $k = \sqrt{2/(H+1)}$ and the phase φ, with $\sin\frac{\gamma}{2} = s_2\,\mathrm{sn}(\varphi/k)$, $\cos\frac{\gamma}{2} = \mathrm{cn}(\varphi/k)$, $w/2 = (s_2/k)\,\mathrm{dn}(\varphi/k)$, $s_2 = \operatorname{sgn} w$ [7, §3.2], and $\varphi_t = \varphi + t$ along a geodesic [7, §3.3]. Sachkov's rotating variables are

$$p = \frac{t}{2k}, \qquad \psi = \frac{\varphi}{k}, \qquad \tau = \psi + p \tag{3}$$

[10, eq. (2.10)]: ψ is the initial phase, τ the midpoint phase, $\psi + 2p$ the terminal phase, and $\dot\theta = -\,\mathrm{cn}(\psi + 2p)$. We write $\mathrm{Exp}(\psi, k, t)$ for the endpoint at time t of the geodesic from the identity with initial data (ψ, k), with $s_2 = 1$ unless the sign is displayed. The other rotating sign acts by $(x, y, \theta) \mapsto (-x, -y, \theta)$ and has the same conjugate times. A geodesic with initial phase ψ is the line $\tau = \psi + p$ in the (p, τ) strip; the source phase has period $4K$, but the conjugate times depend on ψ modulo $2K$ only, so we write $\mathbb{T}_k = \mathbb{R}/2K\mathbb{Z}$ for the phase circle.

The Jacobian. In source variables (t, φ, k) the Jacobian of the exponential map on C_2 is

$$J = -\frac{4k}{(1-k^2)(1-k^2\,\mathrm{sn}^2 p\,\mathrm{sn}^2\tau)}\,J_2, \qquad J_2 = \alpha\,\mathrm{sn}^2\tau + \beta\,\mathrm{cn}^2\tau, \tag{4}$$

with

$$\begin{gathered}\alpha = (1-k^2)\,s\,\alpha_1, \qquad \beta = f_1\beta_1, \qquad f_1 = c\,(\epsilon - p) - d\,s, \qquad \beta_1 = c\,\epsilon - d\,s, \\ \alpha_1 = c\,d\,(p - 2\epsilon) + s\left(d^2 + \epsilon\,(p - \epsilon)\right)\end{gathered} \tag{5}$$

[10, §2.3, eqs. (2.10)–(2.14)]. The denominator satisfies $1 - k^2\,\mathrm{sn}^2 p\,\mathrm{sn}^2\tau \geq 1 - k^2 > 0$. Thus the prefactor is strictly negative on all of C_2, including quarter-period phases. The initial-covector chart is regular: $\det\partial(\gamma_0, w_0)/\partial(\psi, k) = -4/k^2$. Consequently the conjugate times are exactly the positive zeros of J_2 along $\tau = \psi + p$. Appendix B independently derives the signed determinant and records the coordinate changes. Appendix C verifies the hypotheses of the classical second-variation criterion in the fixed-time energy formulation. We write $q = p - \epsilon > 0$ [7, Lemma 5.1] and

$$X = s\,\alpha_1, \qquad \ell = \epsilon\,q > 0 \quad (p > 0). \tag{6}$$

Maxwell roots and the known bracket. We call the positive zeros of the Maxwell equation $f_1 = 0$ the Maxwell roots. At $p = p_n^1$ a point belongs to the reflection-generated Maxwell stratum MAX^2 only when $\mathrm{sn}\,\tau \neq 0$ [7, Proposition 5.2(2), Theorem 5.2(2)]; when $\mathrm{sn}\,\tau = 0$, the reflected source coincides with the original source and $J_2 = 0$. Thus the term "Maxwell cell" below names an interval between these roots, without asserting a Maxwell intersection for every phase at its endpoints. The function f_1 has exactly one zero p_n^1 in each interval $((2n-1)K, (2n+1)K)$, $n \geq 1$, and $(2n-1)K < p_n^1 < 2nK$ [7, Lemma 5.3, Corollary 5.1]; the cut time on C_2 is $t_{\mathrm{cut}} = 2kp_1^1$ [10, Theorem 3.3], equality in the Maxwell bound of [7, Theorem 5.4]. We write $p_0 = p_1^1$. Let $p_1^{\alpha_1}$ be the first zero of α_1 in (p_0, ∞) and

$$p_1 = \min\{2K,\, p_1^{\alpha_1}\}. \tag{7}$$

Sachkov proved that no conjugate time precedes $2kp_0$ and that $t^1_{\mathrm{conj}} \leq 4kK$ [10, Theorems 2.2, 2.3], and stated, with the words "one can show", the sharper bracket

$$2kp_0 \leq t^1_{\mathrm{conj}}(\psi, k) \leq 2kp_1 \tag{8}$$

[10, eq. (2.18)], whose upper endpoint switches at the modulus

$$2E(k_0) = K(k_0), \qquad k_0 = 0.90890855754854147823611890 87\ldots, \tag{9}$$

the unique root of $2E = K$ [9, Proposition 11.5]: $p_1 = 2K$ for $k \le k_0$ and $p_1 = p_1^{\alpha_1} < 2K$ for $k > k_0$; Lemma 3.1(iv) proves this placement, and Theorem 3.4 contains (8). The lower bound in (8) is attained exactly at $\psi \equiv -p_0$ modulo $2K$ [10, Proposition 2.2(1)–(2)]. The n-th Maxwell cell is $[p_n^1, p_{n+1}^1)$; the interval $(0, p_1^1)$ before it carries no conjugate time (Theorem 3.4).

3 The Riccati one-cover

Lemma 3.1 (Identities)**.** *For $0 < k < 1$:*

(i) $\beta = X - \ell$, $\alpha = (1-k^2)X$, $\alpha - \beta = \ell - k^2 X$.

(ii) Wherever defined,

$$\Big(\frac{f_1}{c}\Big)' = -\frac{d^2}{c^2}, \qquad \Big(\frac{\beta_1}{c}\Big)' = -\frac{(1-k^2)s^2}{c^2}, \qquad \Big(\frac{\alpha_1}{d}\Big)' = -\frac{\epsilon f_1}{d^2}.$$

(iii) With $\Gamma = \epsilon - k^2 sc/d$: $\Gamma' = (1-k^2)/d^2 > 0$, $\Gamma(0) = 0$, and $\beta_1' = -s\,d\,\Gamma$.

(iv) Consequently: $f_1 < 0$ on $(0, p_1^1)$ and f_1 has the sign $(-1)^{n+1}$ on (p_n^1, p_{n+1}^1). β_1 has exactly one zero b_n in each $(2nK, (2n+1)K)$, $n \ge 1$, none in $(0, 2K]$ nor in $[(2n-1)K, 2nK]$, and the sign $(-1)^n$ on (b_{n-1}, b_n), $b_0 = 0$. On each cell (p_n^1, p_{n+1}^1) the quotient α_1/d is strictly monotone; α_1 has exactly one zero p_n^α in (p_n^1, b_n), simple, and since $\alpha_1(2nK) = (-1)^n 2n(K-2E)$, it lies in $(2nK, b_n)$ for $k < k_0$, at $2nK$ for $k = k_0$, and in $(p_n^1, 2nK)$ for $k > k_0$. In particular $p_1^\alpha = p_1^{\alpha_1}$, and $p_1 = 2K$ for $k \le k_0$, $p_1 = p_1^{\alpha_1} < 2K$ for $k > k_0$, as stated after (9).

Proof. (i) From (5), $f_1 = -cq - ds$ and $\beta_1 = c\epsilon - ds$; multiplying and using $c^2 + s^2 = 1$, $f_1\beta_1 = s\{cd(q-\epsilon) + s(d^2 + \epsilon q)\} - \epsilon q = X - \ell$. The second identity is the definition of α; subtracting gives the third.

(ii) With $f_1 = -c(p-\epsilon) - ds$ one finds $f_1' c - f_1 c' = -d^2$; with $\beta_1 = c\epsilon - ds$, $\beta_1' c - \beta_1 c' = -(1-k^2)s^2$; and with α_1 as in (5), $\alpha_1' d - \alpha_1 d' = -\epsilon f_1$ after reduction by $c^2 = 1 - s^2$, $d^2 = 1 - k^2 s^2$. The first two identities are [7, Lemma 5.3] and [10, Lemma 2.6] in disguise. The third is derived directly above and supplies the cellwise monotonicity used below.

(iii) $\Gamma' = d^2 - k^2\big[(c^2 - s^2)d^2 + k^2 s^2 c^2\big]/d^2 = \big[d^4 - k^2(1 - 2s^2 + k^2 s^4)\big]/d^2 = (1-k^2)/d^2$, and $\beta_1' = -sd\epsilon + cd^2 + k^2 s^2 c - cd^2 = -sd\,(\epsilon - k^2 sc/d)$.

(iv) By (ii), f_1/c decreases on each $((2m+1)K, (2m+3)K)$ from $+\infty$ to $-\infty$ (there cn has the sign $(-1)^{m+1}$, and $f_1 = (-1)^{m+1}k'$ at the left end, $(-1)^m k'$ at the right end), so the zeros of f_1 are simple and its sign alternates between consecutive zeros; $f_1(0) = 0$ and $f_1(2nK)/\operatorname{cn}(2nK) = 2n(E-K) < 0$ place the sign. For β_1: by (iii) it is strictly monotone on each $(nK, (n+1)K)$, with $\beta_1(2nK) = (-1)^n 2nE$ and $\beta_1((2n+1)K) = (-1)^{n+1}k'$, so it has one zero in $(2nK, (2n+1)K)$ and none in $[(2n-1)K, 2nK]$; on $(0, 2K]$ this is [10, Lemma 2.6]. For α_1: by (ii) and the sign of f_1, α_1/d is strictly monotone on each cell, so α_1 has at most one zero per cell. At p_n^1 and at b_n, $\beta = 0$ gives $X = \ell > 0$, so α_1 has the sign of s there: $(-1)^{n+1}$ at $p_n^1 \in ((2n-1)K, 2nK)$ and $(-1)^n$ at $b_n \in (2nK, (2n+1)K)$. Hence α_1 has exactly one zero in (p_n^1, b_n), simple because $(\alpha_1/d)' \neq 0$ there. Its side of $2nK$ follows from $\alpha_1(2nK) = (-1)^n 2n(K-2E)$, read off from (5) with $s = 0$, $c = (-1)^n$, $d = 1$, $\epsilon = 2nE$, since $2E - K$ decreases strictly from $\pi/2$ to $-\infty$ on $0 < k < 1$ ($dK/dk > 0$ and $dE/dk = (E-K)/k < 0$ [8, §19.4]; this is [9, Proposition 11.5]), so that $K - 2E$ has the sign of $k - k_0$. □

Figure 1 shows the three quotients on both sides of k_0.

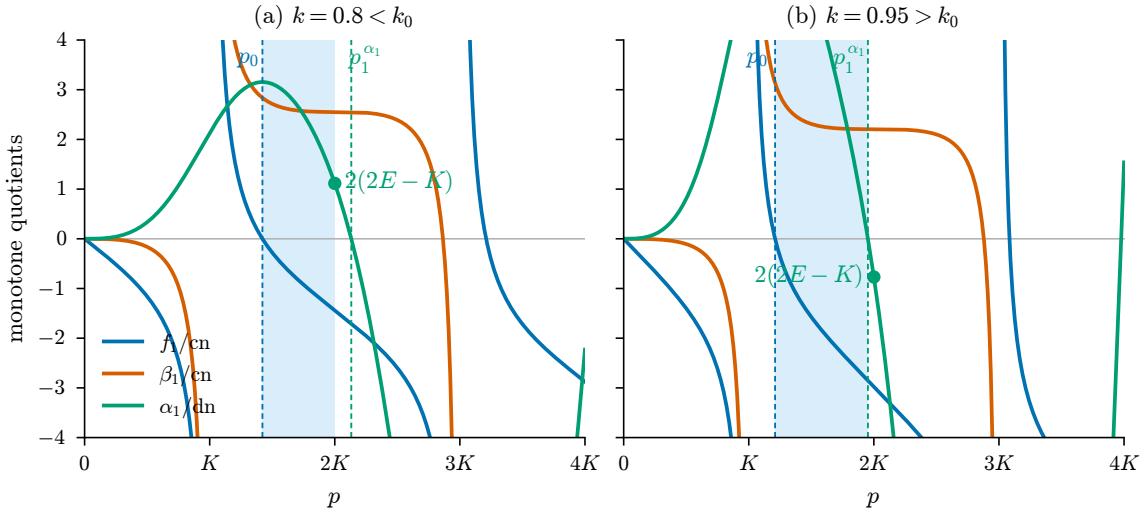


Figure 1: The three cell-wise monotone quotients of Lemma 3.1(ii) for $k = 0.8 < k_0$ (a) and $k = 0.95 > k_0$ (b), against p in units of K; the poles at odd multiples of K are cut at ± 4. The shaded band is the bracket $[p_0, p_1]$. The dot is $\alpha_1(2K) = 2(2E - K)$: positive in (a), so $p_1^{\alpha_1} > 2K$ and $p_1 = 2K$; negative in (b), so $p_1 = p_1^{\alpha_1} < 2K$.

The zero ratio. On an interval where $0 < y := X/\ell < 1$ put

$$z = 1 - y = -\frac{\beta}{\ell}, \qquad \mathsf{D} = 1 - k^2 + k^2 z, \qquad r = -\frac{\beta}{\alpha - \beta} = \frac{z}{\mathsf{D}}, \qquad u = F\big(\arcsin\sqrt{r}, k\big), \tag{10}$$

so that $0 < z, r < 1$ and $0 < u < K$; as $r = (1-y)/(1-k^2 y)$, one has $r \in (0,1)$ exactly when $y \in (0,1)$. Since $\alpha - \beta = \ell\,\mathsf{D} > 0$ by Lemma 3.1(i), the equation $J_2 = (\alpha - \beta)\,\mathrm{sn}^2\,\tau + \beta = 0$ reads

$$J_2 = 0 \iff \mathrm{sn}^2\,\tau = r \iff \tau \equiv \pm u \pmod{2K}. \tag{11}$$

We call r the zero ratio and u its phase lift.

Lemma 3.2 (Riccati slope bound)**.** *For $p > 0$ with $s \neq 0$ put $a = f_1/q$ and $b = -\beta_1/\epsilon$, with z, D as in (10). Then $z = ab$ and*

$$z' = \frac{T_1 + T_2}{d\,s}, \qquad T_1 = d^2\,b\,(1 - z), \qquad T_2 = s^2\,a\,\mathsf{D}, \tag{12}$$

with $T_1 T_2 = d^2 s^2\, z(1-z)\mathsf{D}$. On an interval where $0 < y < 1$, with r, u as in (10), a and b have a common sign, T_1 and T_2 have that sign, and consequently

$$|z'| \geq 2\sqrt{z(1-z)\mathsf{D}}, \qquad |u'| \geq 1, \qquad |u'| - 1 = \frac{(1-k^2)\big(\sqrt{|T_1|} - \sqrt{|T_2|}\big)^2}{2\mathsf{D}^2\,|s|\,d\,\sqrt{r(1-r)(1-k^2 r)}}, \tag{13}$$

so $|u'| = 1$ exactly where $|T_1| = |T_2|$. Moreover, the zeros of $H = T_1 - T_2$ on that interval are simple.

Proof. $ab = -f_1\beta_1/(q\epsilon) = -\beta/\ell = z$ by Lemma 3.1(i); $z \in (0,1)$ forces a common sign of a, b, shared by T_1, T_2 as $1 - z = y > 0$ and $\mathsf{D} > 0$. Using $s' = cd$, $c' = -sd$, $d' = -k^2 sc$, $\epsilon' = d^2$, $q' = k^2 s^2$, direct differentiation gives the Riccati pair

$$a' = \frac{d^2 + ca + k^2 s^2 a^2}{ds}, \qquad b' = \frac{(1-k^2)s^2 - cb - d^2 b^2}{ds}; \tag{14}$$

the mixed terms cancel in $(ab)'$, giving (12). The product $T_1T_2 = d^2s^2\,ab\,(1-z)\mathsf{D}$ and the arithmetic–geometric mean inequality give the first inequality in (13). From (10), $r' = (1-k^2)z'/\mathsf{D}^2$ and $r(1-r)(1-k^2r) = (1-k^2)^2z(1-z)/\mathsf{D}^3$, so $|r'| \geq 2\sqrt{r(1-r)(1-k^2r)}$; and $u' = r'/\big(2\sqrt{r(1-r)(1-k^2r)}\big)$ [8, §19.2(ii)], which gives $|u'| \geq 1$ and, on writing $|T_1| + |T_2| - 2\sqrt{|T_1T_2|}$ as a square, the last identity.

To check equality without an additional finiteness assumption, put $H = T_1 - T_2$, $V = c\mathsf{D} + bd^2$ and $A = 2ak^2s^2 - 2bd^2 - 2ck^2s^2 - c$. The Riccati pair gives

$$H' = \frac{AH - 4as^2V}{ds}. \tag{15}$$

At $H = 0$, the assumption $V = 0$ would imply $c(1-z) + s^2a = 0$, and, on multiplying this relation by bd^2 and using $V = 0$ and the Jacobi first integrals,

$$s^2d^2z - c^2\mathsf{D}(1-z) = (z-c^2)(1-k^2+k^2c^2z) = 0.$$

The second factor is positive; hence $z = c^2$, and $s^2(a+c) = 0$. This contradicts $a + c = -ds/q \neq 0$. Thus $V \neq 0$ at $H = 0$; $a \neq 0$, $s \neq 0$ and (15) give $H' \neq 0$. In particular, the equality set contains no nonempty interval, which already suffices for strict monotonicity of the phase branches used below. Writing $R = z(1-z)\mathsf{D} > 0$, the exact slope gap can also be written as

$$|u'| - 1 = \frac{H^2}{2|ds|\sqrt{R}\big(|T_1| + |T_2| + 2|ds|\sqrt{R}\big)}. \tag{16}$$

At an interior equality point p_t, its denominator equals $8d^2s^2R$. Therefore the gap has a zero of exactly order two there. □

Lemma 3.3 (Crossing principle)**.** *Let $u : [p', p''] \to [0, K]$ be continuous, real-analytic on (p', p'') with $|u'| \geq 1$ there and $|u'|$ unbounded, and with $\{u(p'), u(p'')\} = \{0, K\}$; write $\psi_\sigma(p) = \sigma u(p) - p$, $\sigma = \pm 1$. Then $p'' - p' < K$, and for every $\psi \in \mathbb{T}_k$ the line $\tau = \psi + p$ meets the closed curve $\{\tau \equiv \pm u(p) \pmod{2K},\ p' \leq p \leq p''\}$ in exactly one point: there is exactly one p for which $\psi \equiv \psi_\sigma(p)$ for at least one sign σ. Both signs represent the same point at either endpoint. Consequently $\operatorname{sn}^2(\psi + p) - \operatorname{sn}^2 u(p)$ has exactly one zero in $[p', p'']$. An interior zero is simple except on the branch with $\sigma u'(p) = 1$, where it has odd order at least three. At a corner, $p \in \{p', p''\}$, met exactly for the two corner phases $\psi_\pm(p')$ and $\psi_\pm(p'')$ (the two signs agree there), it is simple provided $\operatorname{sn}^2 u$ has a simple zero at the end where $u = 0$ and $1 - \operatorname{sn}^2 u$ a simple zero at the end where $u = K$. The tangency phases are finitely many when $|u'| \to \infty$ at both ends, or at one end while u extends analytically across the other.*

Proof. Since $|u'| \geq 1$ and u' is continuous, u' has one sign, so $K = |u(p'') - u(p')| = \int_{p'}^{p''} |u'| \geq p'' - p'$, and strictly, since equality would force $|u'| \equiv 1$. The line meets the branch $\tau \equiv \sigma u(p)$ at p if and only if $\psi \equiv \psi_\sigma(p)$. The slopes are $\psi_\sigma' = \sigma u' - 1$; for one sign of σ this is ≤ -2 and for the other it is ≥ 0, and in the latter case ψ_σ is still strictly monotone: it is analytic, and not constant on any subinterval because $|u'|$ is unbounded. The two branches sweep the arcs from $\psi_\sigma(p')$ to $\psi_\sigma(p'')$, of lengths $K - (p'' - p')$ and $K + (p'' - p')$, both less than $2K$; so each branch meets the line at most once, and the arcs tile $\mathbb{T}_k$ once, overlapping only at the two corner phases $\psi_+(p') \equiv \psi_-(p')$ and $\psi_+(p'') \equiv \psi_-(p'')$ modulo $2K$ (the branches meet at $u \in \{0, K\}$), both reached at the same p. Hence every phase is attained exactly once. By (2), $\operatorname{sn}^2(\psi + p) - \operatorname{sn}^2 u(p)$ is $\operatorname{sn}(\psi + p - u)\operatorname{sn}(\psi + p + u)$ times a positive factor, so the order of the zero along the line is that of $\psi_\sigma(p) - \psi$ in the open interval: one where $\psi_\sigma' \neq 0$; at a tangency the slope $\sigma u' - 1 \geq 0$ vanishes to even order, being nonnegative and

analytic, so the zero has odd order at least three; and the zeros of the analytic function $\sigma u' - 1$, which is not identically zero, can accumulate only at an end of the interval, which is excluded where $|u'| \to \infty$ and where u extends analytically across the end. At a corner p_c one expands directly. If $u(p_c) = 0$, the corner phase is $\psi = -p_c$, and, with $h = p - p_c$, $\operatorname{sn}^2(\psi + p) - \operatorname{sn}^2 u(p) = -(\operatorname{sn}^2 u)'(p_c)h + o(h)$, a simple zero when $\operatorname{sn}^2 u$ has a simple zero. If $u(p_c) = K$, the corner phase is $K - p_c$, and $1 - \operatorname{sn}^2(K + h) = (1 - k^2)\operatorname{sn}^2 h / \operatorname{dn}^2 h = O(h^2)$ gives the same conclusion with $1 - \operatorname{sn}^2 u$. □

Theorem 3.4 (Exact first conjugate time)**.** *For every $0 < k < 1$ and every $\psi \in \mathbb{T}_k$ the equation $J_2(\psi + p, p, k) = 0$ has exactly one solution $p_*(\psi, k)$ in $[p_0, p_1]$ and none in $(0, p_0)$; hence*

$$t^1_{\mathrm{conj}}(\psi, k) = 2k\, p_*(\psi, k), \tag{17}$$

and p_* is jointly continuous in k and a local real lift of ψ, the inverse of one of the two branches $\psi \equiv \pm u(p) - p$. Moreover $\min_\psi p_* = p_0$, attained only at $\psi \equiv -p_0$, and $\max_\psi p_* = p_1$, attained only at $\psi \equiv K - p_1$; so $t^1_{\mathrm{conj}} \geq t_{\mathrm{cut}} = 2kp_0$ with equality exactly at $\psi \equiv -p_0 \pmod{2K}$.

Proof. On (p_0, p_1) one has $s > 0$ (as $K < p_0 < p_1 \leq 2K$), $f_1 > 0$ and $\beta_1 < 0$ by Lemma 3.1(iv), and $\alpha_1 > 0$, since $\alpha_1(p_0) > 0$ by Lemma 3.1(iv) and p_1 is at most the first zero of α_1 after p_0; so $\beta < 0 < \alpha$, i.e. $0 < y < 1$; $y = 1$ at p_0 ($\beta = 0$) and $y = 0$ at p_1 ($\alpha = 0$). Thus r runs from 0 to 1, continuously since $\mathsf{D} \geq 1 - k^2$, and $u = F(\arcsin\sqrt{r})$ from 0 to K, continuous on the closed and analytic on the open bracket, with $u' \geq 1$ by Lemma 3.2, and $u' \to \infty$ as $p \to p_0$, because $r(p_0) = 0$ and $r'(p_0) \neq 0$: at the zero p_0 of f_1, $T_1 = d^2 b \neq 0$ in (12). Lemma 3.3 on $[p_0, p_1]$, with (11), gives exactly one root there, continuous in ψ because the branches are strictly monotone. On $(0, p_0)$, $f_1 < 0$ and $\beta_1 < 0$ by Lemma 3.1(iv), so $\beta > 0$ and $\alpha = (1 - k^2)(\beta + \ell) > 0$: $J_2 > 0$, no root (this is [10, Theorem 2.2]). The corner phases are $\psi_\pm(p_0) = -p_0$ and $\psi_\pm(p_1) = K - p_1$, where $p_* = p_0$ and $p_* = p_1$; every other phase is attained at an interior p. The cut time is $2kp_0$ [10, Theorem 3.3].

For joint continuity, the simple zeros defining $p_0(k)$ and $p_1^{\alpha_1}(k)$ vary continuously by the implicit function theorem. Indeed, at a zero of f_1 one has $f_1' = -d^2/c \neq 0$, and at the cell zero of α_1 one has $\alpha_1' = -\epsilon f_1/d \neq 0$. These zeros remain the same indexed zeros locally, by their uniqueness and placement in Lemma 3.1(iv). Thus $p_1(k) = \min(2K(k), p_1^{\alpha_1}(k))$ is continuous even at k_0. If $(\psi_j, k_j) \to (\psi, k)$, the corresponding roots lie in a common compact interval. Any subsequential limit lies in $[p_0(k), p_1(k)]$ and is a zero of $J_2(\psi + p, p, k)$ by joint continuity of the elliptic functions. Uniqueness identifies that limit with $p_*(\psi, k)$, proving convergence of the whole sequence. This argument includes tangencies and the critical coalescence; it does not assume a simple zero of J_2. □

The minimum and its unique phase modulo $2K$ are precisely [10, Proposition 2.2(1)–(2)]: at $p = p_0$, $\operatorname{sn}(\psi + p_0) = 0$ is equivalent to $\psi \equiv -p_0$. Theorem 3.4 additionally gives uniqueness of the root throughout the bracket and the upper-endpoint phase characterization for every modulus. The sharp upper bound and its switch at k_0 were already stated in [10, eqs. (2.18)–(2.19)]. Figure 2 shows the crossing; Figure 4 the root p_* over the cylinder.

4 Conjugate times in every cell

For $n \geq 1$ let b_n and p_n^α be as in Lemma 3.1(iv) and put

$$B_n^- = \big[p_n^1,\ \min(2nK, p_n^\alpha)\big], \qquad B_n^+ = \big[\max(2nK, p_n^\alpha),\ b_n\big]; \tag{18}$$

for $k = k_0$ the brackets touch at $2nK = p_n^\alpha$. For $n = 1$, $B_1^- = [p_0, p_1]$ is the bracket of Theorem 3.4.

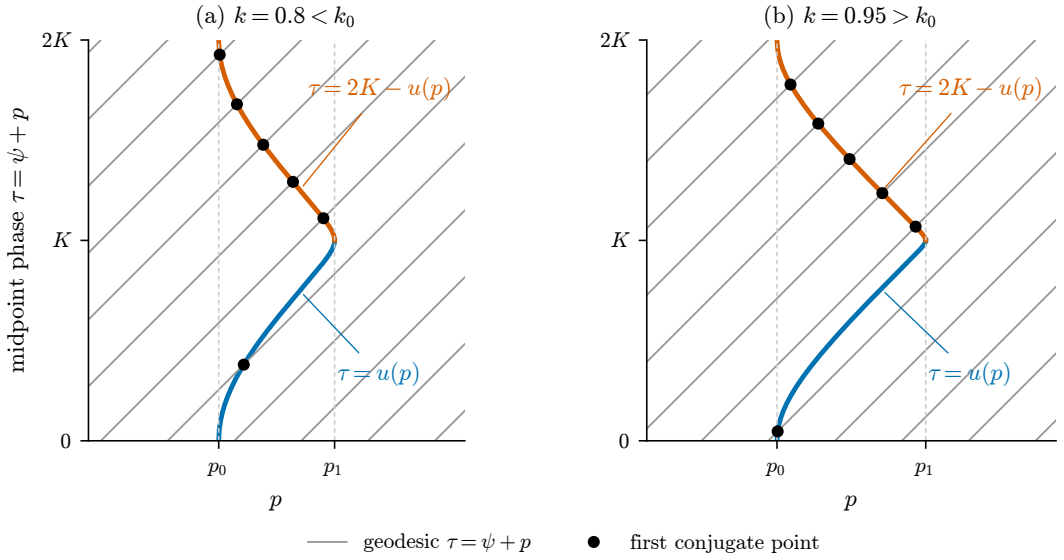


Figure 2: The one-cover in the (p, τ) strip for $k = 0.8$ (a) and $k = 0.95$ (b). The zero set of J_2 is the curve $\tau = u(p)$, of slope at least one, and its mirror $\tau = 2K - u(p)$, of slope at most minus one, for $p_0 \le p \le p_1$. Geodesics are the lines $\tau = \psi + p$ of slope one, wrapped modulo $2K$ and drawn for six initial phases; each meets the curve exactly once, at the marked point. Both axes use equal phase-unit scaling.

Theorem 4.1 (Conjugate times in every cell)**.** *Fix $0 < k < 1$ and $n \ge 1$. Within the cell, $0 < y < 1$, i.e. $0 < r < 1$, exactly on the two open brackets (18), and on each the phase lift u is strictly monotone, from 0 to K on B_n^- and from K to 0 on B_n^+, with $|u'| \ge 1$. Consequently, for every initial phase, the geodesic has exactly one conjugate time on each closed bracket and none elsewhere in $[p_n^1, p_{n+1}^1)$. The two bracket roots are distinct except when $k = k_0$ and $\psi \equiv K \pmod{2K}$: in that case the cell contains the single conjugate time $p = 2nK$. Away from this coalescence the roots are simple except at the interior tangency phases of Lemma 3.3, where their order is exactly three; the coincident root has order four (Remark 4.2). Proposition 4.3 counts the interior tangencies exactly.*

Proof. On (b_n, p_{n+1}^1), f_1 and β_1 have the common sign $(-1)^{n+1}$ by Lemma 3.1(iv), so $\beta > 0$ and $\alpha = (1 - k^2)(\ell + \beta) > 0$: $J_2 > 0$, no zero (there $y > 1$). On (p_n^1, b_n), f_1 and β_1 have opposite signs, so $\beta < 0$; s has the sign $(-1)^{n+1}$ before $2nK$ and $(-1)^n$ after, and α_1 has the sign $(-1)^{n+1}$ before p_n^α and $(-1)^n$ after (Lemma 3.1(iv)). Hence $X = s\,\alpha_1 < 0$ strictly between $2nK$ and p_n^α, where $\beta = X - \ell < 0$ and $\alpha = (1 - k^2)X < 0$ give $J_2 < 0$: no zero (there $y < 0$). On the two open brackets $X > 0$, so $0 < y < 1$, with $y = 1$ at p_n^1 and b_n ($\beta = 0$) and $y = 0$ at $2nK$ and p_n^α ($X = 0$); thus r runs between 0 and 1 and u between 0 and K, from 0 to K on B_n^- and from K to 0 on B_n^+, with $|u'| \ge 1$ (Lemma 3.2) and $|u'|$ unbounded at the end where $r = 0$ (at p_n^1, a zero of f_1, $T_1 = d^2 b \ne 0$; at b_n, a zero of β_1, $T_2 = s^2 a \mathsf{D} \ne 0$); at the other end $r = 1$ and $|u'| \to \infty$ as well, since y has a simple zero there, unless $k = k_0$, where $2nK = p_n^\alpha$, y has a double zero at $2nK$ (as $\alpha_1'(2nK) = (-1)^n 4n^2 E(K - E) \ne 0$). For clarity, set $P = 2nK$ and $h = p - P$ at $k = k_0$. Then $y(P + h) = h^2 + O(h^3)$ and $\mathsf{D}(P) = 1$. The positive square root of $y(P + h)/(\mathsf{D}(P + h)h^2)$ is analytic near zero, with value one. The inverse function theorem applied to $v \mapsto \operatorname{sn} v / \operatorname{dn} v$, whose derivative at zero

is one, therefore gives an analytic $v(h)$ satisfying

$$\frac{\operatorname{sn} v(h)}{\operatorname{dn} v(h)} = h\sqrt{\frac{y(P+h)}{\mathsf{D}(P+h)h^2}}, \qquad v'(0) = 1.$$

The quarter-period identity identifies $K+v(h)$ with $u(P+h)$ for $h < 0$ and with $2K-u(P+h)$ for $h > 0$. This is the analytic continuation needed in Lemma 3.3; hence tangencies cannot accumulate at the critical endpoint either. So Lemma 3.3, with (11), applies to each bracket separately: exactly one root on each closed bracket, simple off the tangency phases, and simple at the corners as well, since $r = \operatorname{sn}^2 u$ and $1 - r$ have the simple zeros just noted, except at the double corner $2nK$ for $k = k_0$. Since $p_n^1 \in B_n^-$ and $b_n < p_{n+1}^1$, these bracket roots exhaust the half-open cell. The roots on the two closed brackets coincide only if both are the common endpoint, which exists only for $k = k_0$, where it is the corner $(2nK, K)$ of both curves, met by the line exactly when $\psi \equiv K - 2nK \equiv K$.

For the interior multiplicity, choose the sign σ with $\sigma u'(p_t) = 1$. Equation (16) and the simple zero of H give

$$\psi_\sigma(p) - \psi_\sigma(p_t) = \frac{H'(p_t)^2}{24d(p_t)^2 s(p_t)^2 R(p_t)}(p - p_t)^3 + O\big((p - p_t)^4\big).$$

Write $C_t > 0$ for this cubic coefficient and $g(\tau) = \operatorname{sn}^2 \tau$. For the tangent phase $\psi = \psi_\sigma(p_t)$, the reduced Jacobian has expansion

$$J_2(\psi + p, p) = -\ell(p_t)\mathsf{D}(p_t)g'(\psi + p_t)C_t(p - p_t)^3 + O\big((p - p_t)^4\big).$$

Indeed $\psi + p = \sigma u(p) - (\psi_\sigma(p) - \psi)$ and $J_2 = \ell\mathsf{D}\{g(\psi + p) - g(\sigma u(p))\}$. Since $g'(\psi + p_t) \neq 0$ for $0 < r(p_t) < 1$, the scalar zero has exactly order three, including the sign of its leading coefficient. □

Remark 4.2. On the open cell (p_n^1, p_{n+1}^1) the count is two except at the corner phase $\psi \equiv -p_n^1$, where the root on B_n^- is the Maxwell root p_n^1 itself, and, for $k = k_0$, at $\psi \equiv K$, where the two roots coincide. That coincident root has scalar order exactly four in every cell. Here is an exact reduction which also describes the noncritical case. For $P = 2nK$, $h = p - P$, and $|h| < K$, put

$$I_k(h) = \int_0^h \frac{\operatorname{sn}^2 v \, \operatorname{dn}^2 v}{\operatorname{cn}^2 v}\, dv.$$

Then

$$J_2(K + P + h, P + h, k) = (1 - k^2)\frac{\operatorname{sn} h \, \operatorname{cn} h}{\operatorname{dn} h}\big\{2n(K - 2E) + I_k(h)\big\}. \tag{19}$$

To verify this, substitute $\epsilon(P + h) = 2nE + \epsilon(h)$ and the Jacobi quarter-period identities into (5). Using $\operatorname{sn}^2 h + \operatorname{cn}^2 h = 1$, the numerator reduces to

$$J_2 \operatorname{dn}^2 h = (1 - k^2)\operatorname{sn} h \, \operatorname{dn} h\big[\operatorname{cn} h\{2n(K - 2E) + h - 2\epsilon(h)\} + \operatorname{sn} h \, \operatorname{dn} h\big].$$

The Jacobi derivatives [8, Table 22.13.1] and $\epsilon' = \operatorname{dn}^2$ give

$$\left(h - 2\epsilon(h) + \frac{\operatorname{sn} h \, \operatorname{dn} h}{\operatorname{cn} h}\right)' = \frac{\operatorname{sn}^2 h \, \operatorname{dn}^2 h}{\operatorname{cn}^2 h}.$$

Both primitives vanish at zero, proving (19). At $k = k_0$ the term containing n vanishes exactly. Since $I_k(h) = h^3/3 + O(h^5)$ and $\operatorname{sn} h \, \operatorname{cn} h / \operatorname{dn} h = h + O(h^3)$,

$$J_2(K + 2nK + h, 2nK + h, k_0) = \frac{1 - k_0^2}{3}h^4 + O(h^6).$$

The integrand is positive for $0 < |v| < K$, so this Jacobian is positive for $0 < |h| < K$ at k_0. For $k \neq k_0$, the root at $h = 0$ is instead simple, with derivative $2n(1-k^2)(K-2E) \neq 0$. For a fixed cell n, the same identity quantifies coalescence as $k \to k_0$. Put $\delta = K - 2E$ and let $x = \sqrt[3]{-6n\delta}$ denote the real cube root. The nonzero root has offset

$$h_n = x + \frac{4k^2-2}{15}x^3 + O(x^5). \tag{20}$$

Indeed, the integrand has expansion $v^2 + (2-4k^2)v^4/3 + O(v^6)$, so $3I_k(h) = h^3 + (2-4k^2)h^5/5 + O(h^7)$, locally uniformly in k. With $b = (4k^2-2)/15$, this reads $x^3 = h^3(1 - 3bh^2 + O(h^4))$. Taking the signed real cube root gives $x = h - bh^3 + O(h^5)$. In particular $h = x + O(x^3)$, and one substitution gives (20). Continuity and strict increase of I_k give existence and uniqueness on both sides of the critical modulus. Since $\delta'(k_0) = E(k_0)/(k_0(1-k_0^2)) > 0$, the separation of the two roots is of order $|k-k_0|^{1/3}$ at fixed n. This explains the sensitivity to rounding the critical modulus; the estimate asserts no uniformity as $n \to \infty$.

These are orders of scalar zeros along a fixed geodesic; they do not by themselves specify the corank or singularity type of the exponential map.

Proposition 4.3 (Number of interior tangencies)**.** *Fix a cell $n \geq 1$. If $0 < k \leq k_0$, neither open bracket has an interior tangency. If $k_0 < k < 1$, each open bracket has exactly one point p_t with $|u'(p_t)| = 1$. It gives one tangent phase $\psi \equiv u(p_t) - p_t$ on B_n^- and $\psi \equiv -u(p_t) - p_t$ on B_n^+, modulo $2K$. Consequently all conjugate roots are simple for $k < k_0$; at $k = k_0$ only the root at $\psi \equiv K$ is multiple, of order four; and for $k > k_0$ the only multiple roots are these interior cubic contacts.*

Proof. Use a, b, H, V from Lemma 3.2 and set $m = k^2$. Throughout (p_n^1, b_n), both c and β_1 have sign $(-1)^n$, while a has sign $(-1)^{n+1}$. The exact factorization

$$V = c\mathsf{D} + bd^2 = \frac{ds}{\epsilon q}\big\{mc\beta_1 + (1-m)q\big\} \tag{21}$$

follows by substituting $a = -c - ds/q$, $b = -c + ds/\epsilon$ and the Jacobi first integrals. Its brace is strictly positive. Thus at every interior zero of H,

$$H' = -\frac{4asV}{d}, \qquad \operatorname{sgn} H' = (-1)^n.$$

There can be at most one such zero per open bracket: all zeros are simple and cross in the same direction, so two would force an intervening crossing in the opposite direction.

It remains to check existence. Put $\chi = (-1)^n$, $P = 2nK$, $\delta = K - 2E$ and $A = E(K-E) > 0$. At p_n^1, $a = 0$ gives $\operatorname{sgn} H = -\chi$; at b_n, $b = 0$ gives $\operatorname{sgn} H = \chi$. At $p_n^\alpha \neq P$, $z = 1$ gives $H = -s^2 a$, of sign χ. At $P + h$, Taylor expansion yields

$$\begin{aligned} H(P+h) &= -\frac{\chi\delta}{2nA}h + O(h^2), \quad k \neq k_0, \\ H(P+h) &= \frac{\chi}{nE}h^3 + O(h^4), \qquad k = k_0. \end{aligned} \tag{22}$$

For the first line, $y(P+h) = \delta h/(2nA) + O(h^2)$, $b(P) = -\chi$, and $s(P+h) = \chi h + O(h^3)$. For the second, $\epsilon(P) = q(P) = 2nE =: B$; substituting $\operatorname{sn} h = h - (1+m)h^3/6 + O(h^5)$, $\operatorname{cn} h = 1 - h^2/2 + O(h^4)$, $\operatorname{dn} h = 1 - mh^2/2 + O(h^4)$ and $\mathcal{E}(h) = h - mh^3/3 + O(h^5)$ into H gives $2\chi h^3/B + O(h^4)$.

For $k < k_0$, the signs at the two ends of the left open bracket are both $-\chi$, and at the ends of the right one both χ; the same is true at $k = k_0$ by the cubic expansion. The common

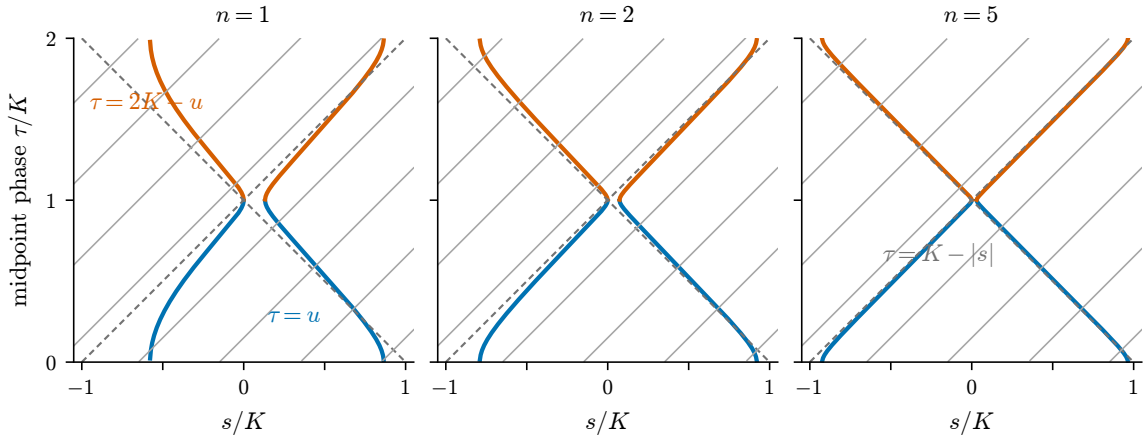


Figure 3: The zero curve of cells $n = 1, 2, 5$ at $k = 0.8$ in the strip, with equal scales on the normalized axes s/K and τ/K, where $s = p - 2nK$: the branch $\tau = u$ (blue) and its mirror $\tau = 2K - u$ (orange) on the two brackets of Theorem 4.1, the broken lines $\tau = K \mp |s|$ of Theorem 5.1(ii) (dashed), and four geodesics, each wrapped modulo $2K$, drawn as lines of slope one. Each line meets the curve once on each bracket; with n the curve straightens onto the broken line and the intersections move to $s = \frac{1}{2}(K - \psi) \bmod K$.

crossing direction excludes interior zeros. For $k > k_0$, the left bracket ends at $p_n^\alpha < P$ and the right begins at P; each has end signs $-\chi, \chi$. The intermediate value theorem gives one zero in each. Only the branch with $\sigma u' = 1$ is tangent there. The multiplicities now follow from Theorem 4.1 and Remark 4.2. □

Figure 3 shows the zero curve of three cells against the offset $s = p - 2nK$, together with its large-index limit from Section 5.

5 The Floquet form of the Jacobian and the large-index law

Let $g(t) = \mathrm{Exp}(\psi, k, t)$ be a rotating geodesic and $T = 4kK$ the period of its body velocity ($2K$ in p). Write $\eta = g^{-1}\partial g$ for the left-trivialized variations with respect to ψ and k, $\xi = g^{-1}\dot{g} = (u_1, 0, u_2)$, and $D(t) = \det[\eta_\psi, \eta_k, \xi]$ for the Jacobian in body coordinates; left trivialization has determinant one and $\partial_\psi = k\,\partial_\varphi$, so D differs from J in (4) by the nonvanishing factor $\pm k$.

Theorem 5.1 (Floquet form and the large-index law)**.** *(i) The period map $h = g(T)$ is a pure translation, of length $L(k) = 4(K - E)$ in the direction of angle $\Phi(\psi, k)$, with $\partial_\psi \Phi = k\,\mathrm{cn}\,\psi$; $g(t + nT) = h^n g(t)$ for $n \geq 0$; and the Jacobian satisfies, exactly,*

$$D(t+nT) = n^2\,\dot{\theta}(t)\,\Delta(\psi,k) + n\,D_1(t) + D(t), \qquad \Delta := \det[\partial_\psi h, \partial_k h] = -k\,L\,L'\,\mathrm{cn}\,\psi, \tag{23}$$

with $L' = 4(dK/dk - dE/dk) > 0$ and $D_1(t) = \det[A_\psi, \eta_k, \xi] + \det[\eta_\psi, A_k, \xi]$, $A = \mathrm{Ad}_{g(t)^{-1}}(h^{-1}\partial h)$. Thus the Jacobian is a quadratic in the number of periods whose leading coefficient vanishes exactly where $\dot{\theta} = -\,\mathrm{cn}(\psi + 2p) = 0$ or $\psi \equiv K$.

(ii) As $n \to \infty$, uniformly for s in compact subsets of $(-K, K)$,

$$\begin{aligned} y(2nK+s) &= \operatorname{sn}^2 s + \frac{(K-2E)\operatorname{sn} s\,\operatorname{cn} s\,\operatorname{dn} s}{2nE(K-E)} + O(n^{-2}), \\ r(2nK+s) &= \operatorname{sn}^2(K-s) + O(n^{-1}), \end{aligned} \tag{24}$$

so the zero curve of cell n tends to $\tau = K - |s|$ and its mirror to $\tau = K + |s|$, and

$$\begin{aligned} p_n^1 &= (2n-1)K + \frac{1}{2n(K-E)} + O(n^{-2}), \qquad b_n = (2n+1)K - \frac{1}{2nE} + O(n^{-2}), \\ p_n^\alpha &= 2nK + \frac{2E-K}{2nE(K-E)} + O(n^{-2}). \end{aligned} \tag{25}$$

For $\psi \not\equiv K$, the conjugate times $p_{(1)} < p_{(2)} < \cdots$ of the geodesic satisfy, uniformly for ψ in compact subsets of $(-K, K)$,

$$p_{(j)} = \left(j + \tfrac{1}{2}\right)K - \tfrac{1}{2}\psi + O(1/j), \tag{26}$$

the two conjugate times of cell n being $p_{(2n-1)}$ and $p_{(2n)}$. At $k = k_0$ the error in (26) improves to $O(j^{-2})$ on the same phase sets. The constants in these estimates can be chosen locally uniformly in $k \in (0,1)$: for the offset and phase estimates, keep s/K and ψ/K in the indicated compact subintervals. No uniformity up to $k = 0, 1$ or up to the excluded phase is asserted.

Part (i) is an exact polynomial-growth identity for parameter variations of a trajectory with periodic body velocity. Its proof uses commuting translation increments and accounts for the parameter dependence of the period; the resulting Jacobian is quadratic in the number of periods. Part (ii) says that the late conjugate times form an arithmetic progression of step K shifted by half the initial phase, because the leading coefficient of (23) vanishes at the inflection points of the planar projection, $\operatorname{sn}(\psi + 2p) = \pm 1$, i.e. $p \equiv \frac{1}{2}(K - \psi) \pmod K$. The excluded phase requires separate indexing: it always has the root $p = 2nK$, but the location of the other root depends on the sign of $K - 2E$; at k_0 the two roots coincide. The exceptional-phase description below makes this distinction explicit.

Proof. (i) Since $\xi(t)$ depends only on the pendulum state it is T-periodic, and $\tilde{g}(t) = g(T)^{-1} g(t+T)$ solves $\tilde{g}' = \tilde{g}\xi$, $\tilde{g}(0) = e$; hence $g(t+T) = h g(t)$ and $g(t+nT) = h^n g(t)$. The rotation part of h is $\theta(T) = -2k \int_0^{2K} \operatorname{cn}(\psi + 2p)\, dp = 0$, so h is a translation, and so is ∂h for either parameter. Differentiating $g(t + nT(\nu); \nu) = h(\nu)^n g(t; \nu)$ along a variation ν of (ψ, k) and left-trivializing, with $\zeta = h^{-1}\partial_\nu h$ (a translation; $\partial_\nu(h^n) = n h^n \zeta$ because translations commute),

$$\eta(t+nT) = \eta(t) + n \operatorname{Ad}_{g(t)^{-1}} \zeta - n T_\nu\, \xi(t);$$

the last term is parallel to ξ and drops out of the determinant; $\operatorname{Ad}_{g(t)^{-1}}$ maps translations to translations by the rotation $R(-\theta(t))$, which preserves planar determinants; and $u_2 = \dot{\theta}$. Expanding $\det[\eta_\psi + nA_\psi, \eta_k + nA_k, \xi]$ gives (23), the n^2 term being $u_2 \det[\zeta_\psi, \zeta_k]$. For Δ: a shift of the initial phase is a shift of time along the same geodesic followed by a left translation, $\operatorname{Exp}(\psi + \delta, k, t) = g(k\delta)^{-1} g(t + k\delta)$, so $h(\psi + \delta) = g(k\delta)^{-1} h(\psi) g(k\delta)$ is $h(\psi)$ rotated by $-\theta(k\delta)$: $|h|$ is independent of ψ and $\partial_\psi \Phi = -k\dot{\theta}(0) = k \operatorname{cn}\psi$. For the length, the translation part of $\operatorname{Exp}(\psi, k, t)$ is $P\, e(a) + Q\, e^\perp(a)$ with $a = \arcsin(k \operatorname{sn}\psi)$, $e(a) = (\sin a, -\cos a)$, $e^\perp(a) = (\cos a, \sin a)$, $P = \int_\psi^{\psi + t/k} k^2 \operatorname{sn}^2 \sigma\, d\sigma$, $Q = k[\operatorname{cn}\psi - \operatorname{cn}(\psi + t/k)]$ [7, §3.3]; at $t = T$ the argument advances by $4K$, so $Q = 0$ and $P = 4(K - E)$. With $h = L\, e_\Phi$,

$e_\Phi = (\cos\Phi, \sin\Phi)$, $e_\Phi^\perp = (-\sin\Phi, \cos\Phi)$, $\det[\partial_\psi h, \partial_k h] = \det[L\Phi_\psi e_\Phi^\perp,\ L' e_\Phi + L\Phi_k e_\Phi^\perp] = -LL'\Phi_\psi$, and $dK/dk > 0 > dE/dk$.

(ii) Put $S = \operatorname{sn} s$, $C = \operatorname{cn} s$, $D = \operatorname{dn} s$, $\epsilon_s = \mathcal{E}(s)$, $q_s = s - \epsilon_s$, $A = E(K-E) > 0$ and $B = Eq_s + (K-E)\epsilon_s$. Quasi-periodicity gives the exact identities

$$\ell(2nK + s) = 4n^2 A + 2nB + \epsilon_s q_s,$$
$$y(2nK + s) - S^2 = \frac{2n(K-2E)SCD + SCD(s - 2\epsilon_s) + S^2D^2}{4n^2A + 2nB + \epsilon_s q_s}.$$

On a compact modulus range and compact normalized offset range the coefficients are bounded and A is bounded below by a positive constant. Expanding this rational expression in $1/n$ proves the first line of (24) with a uniform $O(n^{-2})$ remainder. The map $y \mapsto (1-y)/(1-k^2y)$ has bounded derivative near S^2, since $1 - k^2S^2 = D^2 \geq 1 - k^2 > 0$. Together with $\operatorname{sn}(K - s) = C/D$, this proves the second line. Away from $s = 0, \pm K$, the inverse defining u has bounded derivative, giving $u = K - |s| + O(1/n)$ uniformly on compact sets within the open brackets.

For the endpoints, at $p = 2nK - \sigma$ the equation $f_1 = 0$ reads

$$2n(K-E) = \sigma - \mathcal{E}(\sigma) + \frac{\operatorname{sn}\sigma \operatorname{dn}\sigma}{\operatorname{cn}\sigma}.$$

For $\delta = K - \sigma$ the final quotient is $1/\delta + O(\delta)$. Multiplying the equation by δ/n produces a smooth equation in $(\delta, 1/n)$ with derivative $2(K-E) \neq 0$ at $(0,0)$. The implicit function theorem gives $\delta = 1/(2n(K-E)) + O(n^{-2})$. The equation for b_n is $2nE = \operatorname{sn}\sigma \operatorname{dn}\sigma / \operatorname{cn}\sigma - \mathcal{E}(\sigma)$; the same argument gives $\delta = 1/(2nE) + O(n^{-2})$. Finally, $(-1)^n \alpha_1(2nK + s)/n^2$ extends analytically in $1/n$ to $4A \operatorname{sn} s$, whose derivative at $s = 0$ is $4A > 0$. Its term linear in $1/n$ at $s = 0$ is $2(K - 2E)/n$. The implicit function theorem therefore gives $s = (2E - K)/(2nA) + O(n^{-2})$. The unique indexed zeros from Lemma 3.1(iv) identify these branches with p_n^1, b_n, p_n^α. The nonzero derivatives above are bounded away from zero on compact modulus ranges, giving the stated local uniformity.

The Lean proof gives a direct remainder estimate. After shifting by $2nK$, each endpoint equation has the form $nDg(s) = f(s) + r(s)/n$, where $D > 0$. For the Maxwell and β_1 endpoints take $g = \operatorname{cn}$ with its zero $a = -K$ or $a = K$, respectively. For α_1 take $g = \operatorname{sn}$ and $a = 0$. On the respective windows $|s - a| \leq L|g(s)|$ by the quarter-period identity and concavity of sn on $[0, K]$. Boundedness of f, r first gives $s - a = O(n^{-1})$. Taylor expansion at a now gives $s - a = f(a)/(nDg'(a)) + O(n^{-2})$. Evaluating the three quotients gives (25). The derivative bounds and inverse slopes are uniform on every compact subset of $0 < k < 1$, including sets containing k_0.

For the ordered times write $p = 2nK + s$, $|s| \leq K$. Put $e = \mathcal{E}(s)$, $W = (2nE + e)(2n(K - E) + s - e)$ and $D_s = 1 - k^2 \operatorname{sn}^2 s \operatorname{sn}^2(\psi + s)$. The addition formula for cn in [8, §22.8] factors the determinant at a root as

$$D_s \operatorname{cn}\psi \operatorname{cn}(\psi + 2s) W = \operatorname{dn}^2(\psi + s) R,$$

where, writing $S, C, D = \operatorname{sn} s, \operatorname{cn} s, \operatorname{dn} s$,

$$R = SCD\{s - 2e + 2n(K - 2E)\} + S^2D^2.$$

Both e and $s - e$ are odd and increasing, so $W \geq n^2 E(K-E)$. Also $D_s \geq 1 - k^2$ and $|R| \leq 3K + 1 + 2n|K - 2E|$. Away from the exceptional phase, $\operatorname{cn}\psi$ is bounded below on compact parameter sets. It follows that $\operatorname{cn}(\psi + 2s) = O(n^{-1})$, improving to $O(n^{-2})$ at $K = 2E$. On the left half-cell the argument lies in $[\psi - 2K, \psi]$, containing only the simple

zero $-K$ of cn. On the right it lies in $[\psi, \psi + 2K]$, containing only K. On each window distance to that zero is bounded by a constant times $|\operatorname{cn}(\psi + 2s)|$: divide by distance and extend continuously at the simple zero. Compactness gives a common constant when k stays in a compact subset of $(0, 1)$ and $|\psi|/K \le 1-\eta$ for fixed $\eta > 0$. The two bracket roots therefore have offsets $(-K - \psi)/2$ and $(K - \psi)/2$ up to the stated errors. Theorem 4.1 gives their respective ranks $2n - 1$ and $2n$, proving (26). □

Remark 5.2 (The exceptional phase). For $\psi \equiv K$, the roots in cell n are $2nK$ and $2nK + h_n$, where $h_n \in (-K, K)$ is the unique solution

$$I_k(h_n) = -2n(K - 2E).$$

Indeed, I_k in (19) is odd and strictly increasing, and tends to $\pm\infty$ at $\pm K$; its derivative is positive except at zero. The factor $\operatorname{sn} h \operatorname{cn} h / \operatorname{dn} h$ has only the zero $h = 0$ in this interval. The cell theorem places both roots in the same cell. If $k = k_0$, then $h_n = 0$, and the distinct roots are $p_{(j)} = 2jK$. Otherwise both roots are simple, and

$$h_n = \operatorname{sgn}(2E - K)\left(K - \frac{1}{2n|K - 2E|}\right) + O(n^{-2}).$$

For this estimate, $I_k'(K - \delta) = \delta^{-2} + O(1)$, so $I_k(K - \delta) = \delta^{-1} + O(1)$, and oddness treats the negative end. The remainder is locally uniform away from k_0 and $0, 1$. Thus for $k < k_0$ the ordered roots are $2nK$ followed by $2nK + h_n$; for $k > k_0$ their order is reversed. In the latter case the leading formula (26) happens to hold at the representative $\psi = K$; in the former it holds at $\psi = -K$. Neither observation provides a uniform continuation through the phase-circle boundary or through k_0.

Proposition 5.3 (Late conjugate points are folds)**.** *On every compact subset of* $\{(\psi, k) : 0 < k < 1,\ -K(k) < \psi < K(k)\}$*, there is* n_0 *such that both conjugate points of each cell* $n \ge n_0$ *are folds of the exponential map, for either rotating sign. The phase is represented modulo* $2K$*, with the symmetry described below.*

Proof. We give a direct proof. For a fixed cell index n, use the regular source coordinates (ψ, k, s) defined by $p = 2nK + s$ and $t = 2k(2nK + s)$. The lifted heading is independent of n:

$$\Theta(\psi, k, s) = \arcsin(k \operatorname{sn} \psi) - \arcsin(k \operatorname{sn}(\psi + 2s)),$$
$$\Theta_\psi = k\{\operatorname{cn} \psi - \operatorname{cn}(\psi + 2s)\}, \qquad \Theta_s = -2k \operatorname{cn}(\psi + 2s).$$

Put $A = E(K - E)$, $\Delta_s = 1 - k^2 \operatorname{sn}^2 s \operatorname{sn}^2(\psi + s)$ and $J_n = J_2(\psi + 2nK + s, 2nK + s, k)$. Substitution in (5) and the Jacobi addition formula give the exact polynomial $J_n = n^2 F + nF_1 + F_0$, with

$$F = -4A\Delta_s \operatorname{cn} \psi \operatorname{cn}(\psi + 2s). \tag{27}$$

All coefficients are smooth; their first derivatives are uniformly bounded on compact parameter and offset sets. Thus $J_n/n^2 = F + O(n^{-1})$ in C^1 on such sets, not merely pointwise.

The first variation on the unit energy level gives $\langle \lambda(t), \eta_\psi \rangle = \langle \lambda(t), \eta_k \rangle = 0$ and $\langle \lambda(t), \xi \rangle = 1$, with parameter variations at fixed physical time. To see this directly, for the Liouville form ϑ and the quadratic normal Hamiltonian $\mathcal{H}$ one has $\mathcal{L}_{X_\mathcal{H}} \vartheta = d\mathcal{H}$, hence $\phi_t^* \vartheta = \vartheta + t\, d\mathcal{H}$. Restricting to the initial cotangent fiber and to $\mathcal{H} = 1/2$ gives the two vanishing pairings; homogeneity gives the third. Consequently, whenever $\Theta_\psi \neq 0$ at a conjugate point, the phase column is nonzero and independent of the time column, so the rank is exactly two. The kernel has zero physical-time component and is spanned in (ψ, k, t) by $(\theta_k, -\theta_\psi, 0)$. In the current chart this vector is

$$V_n = (\Theta_k - R_n \Theta_s)\partial_\psi - \Theta_\psi \partial_k + R_n \Theta_\psi \partial_s, \qquad R_n = 2n(K/k + K') + s/k.$$

By (26), the two roots satisfy $s_n^{\pm} = s_\pm + O(n^{-1})$ uniformly, where $s_- = -\frac{1}{2}(K+\psi)$ and $s_+ = \frac{1}{2}(K-\psi)$. At these limits $\Theta_s = 0$, $\Theta_\psi = k\,\mathrm{cn}\,\psi \neq 0$. Using (27) and the C^1 estimate gives, at the roots,

$$\frac{V_n(J_n)}{n^3} = \pm\frac{16E^2(K-E)}{k'}\,\Delta_{s_\pm}\,\mathrm{cn}^2\,\psi + O(n^{-1}), \qquad k' = \sqrt{1-k^2}. \tag{28}$$

Indeed the limiting expression is $2(K/k+K')\Theta_\psi F_s$; here $F_s = 8A\Delta_{s_\pm}\,\mathrm{cn}\,\psi\,\mathrm{sn}(\psi+2s_\pm)\,\mathrm{dn}(\psi+2s_\pm)$, $\psi + 2s_\pm = \pm K$, and $K + kK' = E/(1-k^2)$. The positive magnitude on the right of (28) is bounded below on the prescribed compact set. Thus for all sufficiently large n the rank is two and the kernel derivative of the determinant is nonzero, since the determinant is a smooth nonvanishing factor times J_n. The opposite rotating sign reflects both planar target coordinates and has the same rank and fold type. A phase shift by $2K(k)$ acts on the target by $(x, y, \theta) \mapsto (-x, y, -\theta)$, as follows from Appendix B; this source and target symmetry extends the assertion to every phase off $\psi \equiv K \pmod{2K}$.

For completeness, this rank-and-derivative test gives a fold directly. At rank two, the inverse function theorem puts a map between three-dimensional manifolds in the form $(u_1, u_2, z) \mapsto (u_1, u_2, f(u,z))$. The test is $f_z = 0$, $f_{zz} \neq 0$. Solving $f_z(u, z_0(u)) = 0$ and subtracting $f(u, z_0(u))$ leaves $(z - z_0(u))^2 a(u,z)$ with $a \neq 0$. The smooth coordinate $(z - z_0(u))\sqrt{|a(u,z)|}$ gives the fold normal form $(u_1, u_2, \pm z^2)$. This proof uses neither a global fold certificate nor a scalar-root multiplicity as a substitute for the rank condition. □

Remark 5.4 (Separatrix limits). As $k \to 1$,

$$K\,(p_0 - K) \to 1, \qquad 2K - p_1 \to \operatorname{artanh}\tfrac{1}{2} = \tfrac{1}{2}\ln 3. \tag{29}$$

Indeed $K \to \infty$, $E \to 1$, and uniformly on compact sets $\mathrm{sn} \to \tanh$, $\mathrm{cn}, \mathrm{dn} \to \mathrm{sech}$, $\mathcal{E} \to \tanh$ [8, §22.5(ii)]. With $p = K + x$, $x = \sigma/K$, and the quarter-period shifts [8, §22.4],

$$-\frac{\mathrm{dn}^2\,x}{k'}\,f_1(K+x) = \mathrm{cn}\,x - \mathrm{sn}\,x\,\mathrm{dn}\,x\Big(K + x - E - \mathcal{E}(x) + \frac{k^2\,\mathrm{sn}\,x\,\mathrm{cn}\,x}{\mathrm{dn}\,x}\Big) \to 1 - \sigma$$

uniformly for $0 \le \sigma \le \Sigma$, so the unique zero p_0 of f_1 in $(K, 3K)$ has $K(p_0 - K) \to 1$. With $p = 2K - x$ and the half-period shifts, $\alpha_1(2K-x)/(2K) \to -\operatorname{sech}^2 x + \tanh x\,(2 - \tanh x) = 2\tanh x - 1$ uniformly on compacts, so for $k > k_0$ the unique zero $p_1 = p_1^{\alpha_1}$ of α_1 in $(p_0, 3K)$ has $2K - p_1 \to \operatorname{artanh}\frac{1}{2}$. The rate can be stated more precisely. With $a = \frac{1}{2}\log 3$,

$$K(p_0 - K) = 1 + K^{-1} + O(K^{-2}), \qquad 2K - p_1 = a - \frac{1}{2K} + O(K^{-2}). \tag{30}$$

Here is a justification beyond convergence alone. Write $\delta = 1 - k^2$. The complete-integral expansions [8, §19.12] give $K = \log(4/\sqrt{\delta}) + O(\delta\log(1/\delta))$ and $E = 1 + O(\delta\log(1/\delta))$. The Jacobi ODE has smooth parameter dependence on each fixed finite argument interval; comparison with its $k = 1$ solution gives $O(\delta)$ errors, including first derivatives, for $\mathrm{sn}, \mathrm{cn}, \mathrm{dn}, \epsilon$ there. These errors times any fixed power of K tend to zero. For the lower root $x = p_0 - K = O(K^{-1})$, Taylor expansion of the quarter-period equation above gives $0 = 1 - (K-E)x + O(x^2 + Kx^3)$, uniformly as $k \to 1$. Consequently $x = (K-E)^{-1} + O(K^{-3})$, proving the first estimate. For the upper root, the same parameter comparison gives, uniformly with one derivative near a,

$$\frac{\alpha_1(2K-x)}{2K} = F(x) + \frac{C(x)}{2K} + O(\delta K), \qquad F(x) = 2\tanh x - 1,$$

where, with $t = \tanh x$, $C(x) = (1-t^2)(x+4-t) - t(2-t)(x+2-t)$. At $x = a$, $F(a) = 0$, $F'(a) = 3/2$ and $C(a) = 3/2$. Taylor expansion at this simple root gives the second estimate in (30). Thus the two scaled quantities in (29) approach their limits at order $1/K$, which is logarithmic in $1/(1-k)$.

6 Numerical checks

The proofs are analytic; computation was used to find the statements and to check them independently. The archived later-cell experiment integrates the normal Hamiltonian system in pendulum coordinates together with its variational equations. Neither the flow nor those equations uses elliptic functions or the reduced Jacobian. Zeros of the endpoint-map determinant are sought through sign changes on a sampled time grid. Such a detector can miss even-order contacts, in particular the quartic zero at $k = k_0$, $\psi \equiv K$, proved in Remark 4.2. The analytical counting theorems, rather than the scan, exclude additional roots. A separate reproducible check, `research/e153_contact_check.py`, uses exact polynomial reduction for (19) and an ODE Taylor recurrence for its critical expansion. At 70-digit precision, direct differentiation of the original coefficients checks 18 selected cubic contacts and the quartic coefficient in cells $n = 1, 2, 5, 10$; numerical quadrature also checks the integral identity at 20 noncritical sample points. These are finite checks of local coefficients, not a numerical completeness certificate or a classification of the exponential map's singularities. The local inversion (20) is checked separately by `research/e156_coalescence_check.py`: two exact series reductions and 24 evaluations of the original Jacobian at 80-digit precision, with $n = 1, 5$ and both signs of $k - k_0$ from 10^{-6} to 10^{-21}. For Proposition 4.3, `research/e158_tangency_count_check.py` verifies the factorization (21) and both local expansions (22) symbolically. It independently samples 54 brackets at 65-digit precision, including moduli on both sides of k_0 at distance 10^{-8} and k_0 itself, and checks the cubic Jacobian coefficient at the 24 detected contacts. Completeness comes from the analytic sign argument, not from this finite sample. The separate driver `research/e154_asymptotic_check.py` checks endpoint and phase-root asymptotics at $n = 10, 30, 100$, the exceptional-phase indexing, the first separatrix corrections, and the quadratic Floquet coefficient at 70-digit precision. Exact coefficient reductions are recorded in `research/e154_asymptotic_algebra.py`; sampled remainders do not prove uniform error estimates, which are supplied analytically above. For Proposition 5.3, `research/e155_late_fold_check.py` differentiates the original endpoint at 36 late roots and both rotating signs, checks the first-variation pairings and the kernel relation, and compares the direct physical-time derivative with (28). Its companion exact-algebra script verifies (27). These finite 65-digit checks corroborate the analytic proof; the uniform conclusion comes from its compactness bounds.

The retained later-cell output contains 720 distinct records. It uses twelve initial phases, both rotating signs, five moduli and six cells:

$$\frac{\psi}{2K} = \frac{j + 0.37}{12} \ (j = 0, \dots, 11), \qquad k \in \{0.3, 0.6, 0.85, 0.95, 0.99\}, \qquad n = 1, \dots, 6.$$

Each record reports two detected roots, one per bracket of (18), and none in the gap or tail. These are 120 distinct geodesics; the sign-change detector cannot exclude unresolved contacts. The identities of Lemmas 3.1 and 3.2 were checked symbolically and in 30-digit arithmetic.

The archived large-index check uses finite sets of indices. At $k = 0.6, 0.95$, respectively, the absolute remainders of (25) multiplied by n^2 are below $(0.73, 0.18, 0.42)$ and $(0.20, 0.23, 0.003)$, in endpoint order (p_n^1, b_n, p_n^α), for $n \in \{2, 5, 10, 20, 40\}$. For $n \in \{5, 20, 80\}$ and $s/K \in \{-0.6, -0.2, 0.3, 0.7\}$, $n|y(2nK + s) - \operatorname{sn}^2 s|$ is below 0.53 and 0.046. For six phases $\psi/(2K) = (j + 0.3)/6$, $j = 0, \dots, 5$, the roots in cells 5 and 20 differ from (26) by less than $(0.073K, 0.010K)$ at $k = 0.6$ and $(0.0062K, 0.0009K)$ at $k = 0.95$. These are sampled discrepancies, not bounds for all intermediate indices or phases; the error estimates in Section 5 are analytic.

The archived ODE Floquet experiment uses $k = 0.7$, $\psi/(2K) = 0.37$, and times $t_0 + 2nT$, $n = 0, \dots, 10$, with $t_0/(2T) \in \{0.05, 0.13, 0.20, 0.26, 0.40, 0.56, 0.70, 0.90\}$. It measures the determinant in (γ_0, c_0, t) coordinates, which differs from D by a constant nonzero source-coordinate factor along the fixed geodesic. The quadratic fit has residual below 10^{-9}; the ratio of its leading coefficient to $\dot{\theta}(t_0)$ is constant to the four decimal places recorded. Sampling every two periods is consistent with (23), but is not a check at odd period shifts.

Figure 4 uses a finite phase–modulus grid with the `elliptic-functions` package [5]: 152 moduli, approximately $0.000400 \le k \le 0.999996$, and 256 phases. The array stores 38,912 roots and their normalized values; it does not cover the limiting moduli. Its fixed-modulus profiles illustrate the phase dependence first plotted in [10, Figures 5–7]. The independent 60-digit audit `research/e156_numerical_provenance.py` reconciles the stored later-cell records and checks 60 entries of this array against original elliptic formulas. The largest normalized root discrepancy is 2.51×10^{-5} near the rounded critical modulus; the other 59 discrepancies are below 1.70×10^{-9}. The critical coalescence is sensitive to rounding k_0, so a small determinant residual alone is not a root-error bound there. The revised first-root solver refines in the time coordinate and uses higher precision near the critical corner. A regression in `tests/test_jacobian.py` compares both public first-root routines with four high-precision roots, including a rounded quarter period. This audit does not replay the historical ODE runs or certify the unsampled continuum.

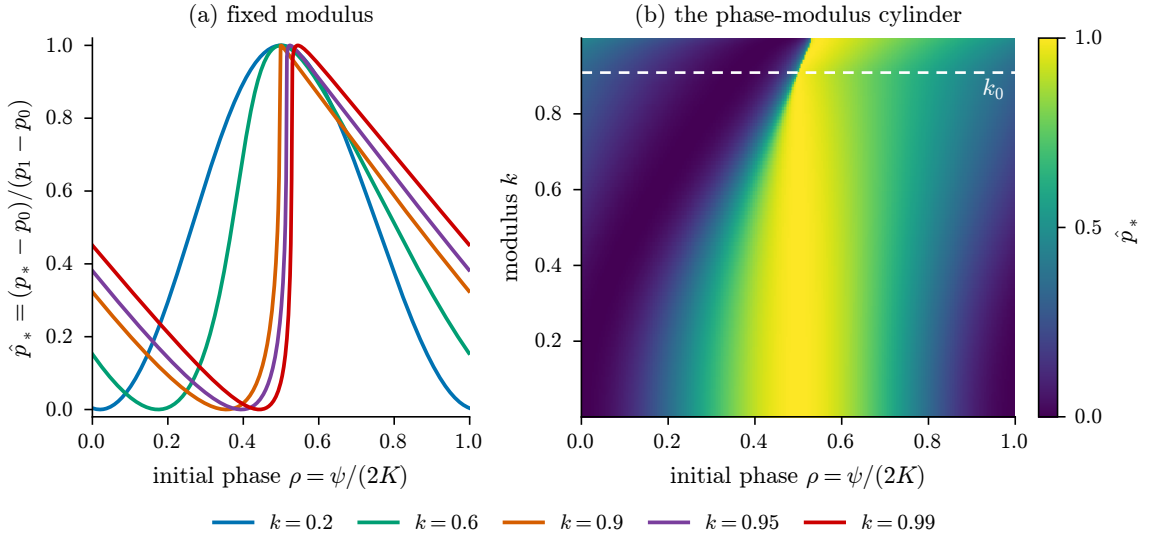


Figure 4: The normalized first conjugate root $\widehat{p}_* = (p_* - p_0)/(p_1 - p_0)$ against the phase $\psi/(2K)$. (a) Five fixed-modulus profiles, $k = 0.2, 0.6, 0.9, 0.95, 0.99$. (b) The phase–modulus cylinder, $\psi/(2K)$ horizontal, k vertical, colored by $\widehat{p}_*$; the dashed line is the critical modulus k_0. The color scale is normalized separately at each modulus by the exact endpoints.

Code and data availability

The integration, formula checks and figure-generation code are at `https://github.com/moiseevigor/se2-conjugate-locus`: `scripts/review/indep_ode.py`, `scripts/review/referee_formula_check.py` (first cell); `scripts/review/indep_ode_higher.py` (critical contact); `research/e6_later_cells_ode.py` (later cells); `research/e_a5_`

`large_n.py`, `research/e11_lemma_check.py`, `research/e15_drift_map.py` (large index, Floquet form, drift map); `scripts/review/separatrix_limit.py` (separatrix); `scripts/manuscript_figures.py`, `scripts/higher_figures.py` (figures).

The figure-data audit and rendering driver are `research/e156_numerical_provenance.py` and `research/e156_figure_audit.py`; their JSON outputs and source hashes are retained under `data/` and `references/e156/`.

Stored later-cell results are in `research/e6_later_cells_ode.json`; large-index and Floquet summaries are in `data/e79_large_index_check.txt` and `data/e79_floquet_check.txt`. The review evidence in `references/review_2026-09-20_article1/` records the exact symbolic checks, separate 60-digit endpoint and limit checks, and the fresh Lean validation, with their respective scopes.

The counting proofs of Sections 3–4 are formalized in Lean 4 with Mathlib in `lean/`. The abstract interfaces specify $\mathrm{sn}, \mathrm{cn}, \mathrm{dn}, \mathcal{E}$ through their derivative rules and algebraic relations, their values at the multiples of K and signs between them, $0 < E < K$, the inverse phase lift $F(\arcsin\sqrt{r})$ and the characterization $\mathrm{sn}^2 x = \mathrm{sn}^2 y \iff x \equiv \pm y \pmod{2K}$. A concrete real inverse-integral construction instantiates these interfaces. The identities of Lemma 3.1, the Riccati pair and the slope bound $|u'| \geq 1$, the sign chart, the crossing count of Lemma 3.3, the uniqueness in Theorem 3.4 with the absence of conjugate times before p_0, and in Theorem 4.1 one root per closed bracket, none elsewhere in the cell, the contact of the brackets exactly at $K = 2E$, the coincidence only at $p = 2nK$ for $\psi \equiv K$, and the total of $2N$ conjugate times before p^1_{N+1} for $K \neq 2E$, are theorems there as statements about the scalar function J_2. Appendix A explains the construction, the formal theorems and the remaining scope limits.

A Scope of the Lean formalization

The development in `lean/` (37 modules, Lean 4.33.1, Mathlib revision `0df444a`, no `sorry`, axioms `propext`, `Classical.choice`, `Quot.sound`) constructs the real Jacobi functions from the inverse elliptic integral. The reusable structure `JacobiFull` has 31 conditions, listed in Table 1; `Reduction` derives them from the 13 conditions of `JacobiCore` in Table 3. The module `Construction` supplies a concrete `JacobiCore` for every $0 < k < 1$, proving all its other conditions, including the existence and first-zero property of K. Thus the concrete counting results assume neither Jacobi-function existence nor a separate first-zero hypothesis. Every other object of the proofs (the Maxwell times p^1_n as the zeros of f_1, the zeros b_n of β_1, the bracket ends, the signed brackets `SBracket` and the crossing data `CrossingData` of Lemma 3.3) is constructed inside Lean and its properties are proved there. Beyond these fields, the counting theorems take no additional tangency-finiteness hypothesis: `Tangency` proves (15) and the nonvanishing of H' at $H = 0$ from the same Jacobi data, excluding any interval of equality in the slope bound. This is enough for `SignedTime.psiP_strictMono`, and hence for all counting results. Table 2 names the formal theorems and the statements of the article they prove. The value $\mathrm{dn}(2nK) = 1$, used in Lemma 3.1(iv), is not assumed: it follows from `sd` and `s_even`.

Table 1: The 31 conditions of `JacobiFull`, grouped by interface. Classical justifications are listed; `Construction` and `Reduction` prove every condition beyond $0 < k < 1$.

Condition	Field(s)	Classical justification
`JacobiData`: derivative rules and algebraic relations		
$0 < k < 1$	`k_pos`, `k_lt_one`	the modulus of C_2, Section 2
$\mathrm{sn}' = \mathrm{cn}\,\mathrm{dn}$, $\mathrm{cn}' = -\mathrm{sn}\,\mathrm{dn}$, $\mathrm{dn}' = -k^2\,\mathrm{sn}\,\mathrm{cn}$	`hs`, `hc`, `hd`	[8, §22.13(i)]
$\mathcal{E}' = \mathrm{dn}^2$	`heps`	definition of $\mathcal{E}$, Section 2; [8, §22.16(ii)]
$\mathrm{cn}^2 + \mathrm{sn}^2 = 1$, $\mathrm{dn}^2 = 1 - k^2\,\mathrm{sn}^2$	`sc`, `sd`	[8, §22.6(i)]
`JacobiInit`: values at 0		
$\mathrm{dn} > 0$	`d_pos`	$\mathrm{dn} \geq k' > 0$ for $0 < k < 1$
$\mathrm{sn}\,0 = 0$, $\mathrm{cn}\,0 = 1$, $\mathcal{E}(0) = 0$	`s0`, `c0`, `eps0`	[8, §22.4]
`JacobiPeriodic`: values at the multiples of K and signs between them		
$0 < E < K$	`K_pos`, `E_pos`, `E_lt_K`	$K - E = k^2 \int_0^K \mathrm{sn}^2 > 0$
$\mathrm{sn}(2nK) = 0$, $\mathrm{sn}((2n+1)K) = (-1)^n$, $\mathrm{cn}(2nK) = (-1)^n$, $\mathrm{cn}((2n+1)K) = 0$, $\mathrm{dn}((2n+1)K) = k'$	`s_even`, `s_odd`, `c_even`, `c_odd`, `d_odd`	[8, §22.4]
$\mathcal{E}(nK) = nE$	`eps_even`, `eps_odd`	$\mathcal{E}(u + 2K) = \mathcal{E}(u) + 2E$ and $\mathcal{E}(K) = E$, [8, §22.16(ii)]
sn has the sign $(-1)^n$ on $(2nK, (2n+2)K)$; cn has the sign $(-1)^{n+1}$ on $((2n+1)K, (2n+3)K)$	`s_sign`, `c_sign`	the zeros of sn, cn are simple and lie at $2nK$, $(2n+1)K$, [8, §22.4]
`JacobiFull`: the phase lift		
$F(\arcsin\sqrt{r})$: continuous on $[0,1]$, $0 \mapsto 0$, $1 \mapsto K$, derivative $1/(2\sqrt{r(1-r)(1-k^2r)})$ on $(0,1)$, $\mathrm{sn}^2(F(\arcsin\sqrt{r})) = r$	`Finv_cont`, `Finv_zero`, `Finv_one`, `Finv_deriv`, `Finv_spec`	the lift u of (10); [8, §19.2(ii)]
$\mathrm{sn}^2 x = \mathrm{sn}^2 y \iff x \equiv \pm y \pmod{2K}$	`sn_sq_eq_iff`	(2) and the zeros of sn, [8, §22.4]

Table 2: Formal theorems and the statements they prove. Cell m of the Lean development is the cell $n = m + 1$ of the article.

Lean theorem (module)	Statement
`collapse_beta`, `collapse_alpha`, `collapse_diff`, `hasDerivAt_f1_div_c`, `hasDerivAt_`β_1`_div_c`, `hasDerivAt_`α_1`_div_d` (`Identities`)	Lemma 3.1(i), (ii)
`exists_unique_f1_zero`, `f1_sign_before`, `f1_sign_after` (`ZerosF1`); `exists_unique_`β_1`_zero` (`Zeros`); `signed_`α_1`_div_d_strictAntiOn`, α_1`_even` (`CellCount`)	Lemma 3.1(iv): the zeros and signs of f_1 and β_1, the monotone quotient $\alpha_1/\operatorname{dn}$, $\alpha_1(2nK) = (-1)^n 2n(K - 2E)$
`a_deriv_form`, `b_deriv_form`, `T1_T2_same_sign`, `slope_bound_abs` (`Riccati`); `one_le_`ε`_deriv_u` (`SignedBracket`)	Lemma 3.2: the Riccati pair (14), $\lvert z'\rvert \geq 2\sqrt{z(1-z)\mathsf{D}}$ and $\lvert u'\rvert \geq 1$
`hasDerivAt_H`, `V_ne_of_H_zero`, `Hp_ne_of_H_zero` (`Tangency`)	Equation (15) and the simplicity of the interior zeros of H
`H_zero_of_unit_slope`, `no_interval_H_zero` (`Tangency`); `psiP_strictMono` (`SignedTime`)	Equality in the slope bound forces $H = 0$; no interval of equality; strict monotonicity without a separate tangency assumption
`crossing` (`Crossing`)	Lemma 3.3, counting clause: for every ψ exactly one $p \in [p', p'']$ with $\psi \equiv \psi_\sigma(p)$ for some sign σ
`J2_eq_zero_iff`, `exact_time` (`SignedTime`)	(11) on a bracket and one zero of J_2 on each closed bracket, for both orientations of u
`J2_pos_before_p0`, `exact_first_time`, `first_time_complete` (`BeforeFirst`)	Theorem 3.4: no zero in $(0, p_0)$, exactly one in $[p_0, p_1]$, hence exactly one in $(0, p_1]$
`eL_eq_eR_iff`, `two_per_cell_of_ne`, `coincide_imp` (`CellCount`)	Theorem 4.1: the brackets touch exactly when $K = 2E$; two zeros in $[p_n^1, p_{n+1}^1)$ when $K \neq 2E$; in general the zero set of the cell is $\{p, q\}$ with $p \in B_n^-$, $q \in B_n^+$
`J2_even_eq_zero_iff` (`BeforeFirst`)	$J_2(\tau, 2nK) = 0 \iff \tau \equiv K \pmod{2K}$: the coincident root $p = 2nK$ occurs only for $\psi \equiv K$
`roots_ncard` (`BeforeFirst`)	$2N$ zeros in $(0, p_{N+1}^1)$ for $K \neq 2E$

The reduced hypothesis surface. The module `Reduction` defines a structure `JacobiCore` with the 13 hypotheses of Table 3 and constructs from it an instance of `JacobiFull` (`JacobiCore.toJacobiFull`), so that the 18 remaining fields of Table 1 are theorems. The algebraic relations are first integrals of the differential system; $\operatorname{dn} > 0$ follows from $\operatorname{dn}^2 \geq 1 - k^2$ and $\operatorname{dn}(0) = 1$ by the intermediate value theorem; the values at the multiples of K and the sign clauses follow from the reflection $u \mapsto 2K - u$ and the shift $u \mapsto u + 2K$, which are consequences of uniqueness for the differential system (the squared distance of two bounded solution triples satisfies $|\Phi'| \leq 4\Phi$, so Gronwall's inequality, `eq_zero_of_abs_deriv_le_mul_abs_self_of_eq_zero_right` in Mathlib, gives $\Phi \equiv 0$); $E := \mathcal{E}(K)$ satisfies $0 < E < K$ because $\mathcal{E}' = \operatorname{dn}^2 > 0$ and $(p - \mathcal{E})' = k^2 \operatorname{sn}^2 > 0$ on $(0, K)$; the phase lift $F(\arcsin\sqrt{r})$ is constructed as the inverse of sn^2 on $[0, K]$, with its derivative from the inverse function rule and its continuity from the strict monotonicity; and $\operatorname{sn}^2 x = \operatorname{sn}^2 y \iff x \equiv \pm y \pmod{2K}$ from the oddness of sn, the $2K$-periodicity of sn^2 and the injectivity of sn^2 on $[0, K]$.

Concrete construction. For $0 < k < 1$ define the oriented real integrals

$$F_k(\varphi) = \int_0^\varphi \frac{dt}{\sqrt{1 - k^2 \sin^2 t}}, \qquad G_k(\varphi) = \int_0^\varphi \sqrt{1 - k^2 \sin^2 t}\, dt.$$

Since $0 < 1 - k^2 \sin^2 t \le 1$, we have $F_k' \ge 1$. Thus F_k is strictly increasing, with $F_k(\varphi) \ge \varphi$ for $\varphi \ge 0$ and $F_k(\varphi) \le \varphi$ for $\varphi \le 0$; the intermediate value theorem makes it a bijection of $\mathbb{R}$. Let $\phi_k = F_k^{-1}$ be its unwrapped real inverse. The definitions

$$s(p) = \sin \phi_k(p), \quad c(p) = \cos \phi_k(p), \quad d(p) = \sqrt{1 - k^2 s(p)^2}, \quad \mathcal{E}(p) = G_k(\phi_k(p))$$

satisfy all four differential equations and initial values by the inverse function rule and the fundamental theorem of calculus. Moreover, $K = F_k(\pi/2) > 0$, $c(K) = 0$ and $c > 0$ on $[0, K)$, while $E = \mathcal{E}(K) = G_k(\pi/2)$. These are the classical real Jacobi functions [8, §19.2(ii), §22.16]; the contribution here is their formal construction, not a new special-function identity.

In the namespace `JacobiConcrete`, `core` and `full` construct the two interfaces; `full_K` and `full_E` identify their constants with the complete elliptic integrals. The exported `first_time_unique` needs only $0 < k < 1$ and the phase. The exported `two_per_cell` and `roots_ncard` additionally require $F_k(\pi/2) \neq 2G_k(\pi/2)$, preserving the critical-modulus exception. Their axiom audit uses only the three logical axioms listed above. An independent numerical comparison of quadrature and inversion with SciPy's Jacobi functions agrees in 72 samples, including negative and multi-period amplitudes, to absolute error below 1.1×10^{-13} (`research/e144_inverse_integral_check.py`); this is sampled corroboration, whereas Lean proves the global construction.

Table 3: The 13 conditions of `JacobiCore`. `Construction` proves them from $0 < k < 1$; `Reduction` then constructs `JacobiFull`.

Condition	Field(s)
$0 < k < 1$	`k_pos`, `k_lt_one`
$\mathrm{sn}' = \mathrm{cn}\,\mathrm{dn}$, $\mathrm{cn}' = -\mathrm{sn}\,\mathrm{dn}$, $\mathrm{dn}' = -k^2\,\mathrm{sn}\,\mathrm{cn}$, $\mathcal{E}' = \mathrm{dn}^2$	`hs`, `hc`, `hd`, `heps`
$\mathrm{sn}\,0 = 0$, $\mathrm{cn}\,0 = 1$, $\mathrm{dn}\,0 = 1$, $\mathcal{E}(0) = 0$	`s0`, `c0`, `d0`, `eps0`
$K > 0$, $\mathrm{cn}\,K = 0$, $\mathrm{cn} > 0$ on $[0, K)$	`K_pos`, `cK`, `c_pos`

The module `Endpoint` verifies the concrete endpoint formulas against all five pendulum/horizontal equations, their zero-time endpoint, and unit control norm for either rotation sign. It also proves positivity of the denominator in (4) and equivalence of zeros for its scalar right-hand side and J_2. The distinction matters: `jacobianExpression` denotes that expression, not a formally computed endpoint determinant. The theorem `JacobiConcrete.endpoint_hamiltonian_system` combines the five trajectory equations without an extra trajectory hypothesis.

The module `Modulus` proves the modulus derivatives of the real first- and second-kind integrals for every $0 < k < 1$ and every real amplitude. It supplies local uniform bounds for differentiation under the integral, evaluates the derivative integrals by the fundamental theorem of calculus, and proves joint strict Fréchet differentiability in modulus and amplitude. The coordinate order is (k, a): differentiation is in the modulus k, not the parameter $m = k^2$. The complete-integral derivative formulas follow at $a = \pi/2$. These are formal reproductions of classical identities, not new special-function results. The 16-declaration audit uses only the standard logical axioms. Independent 50-digit checks of 48 modulus and 48 joint directional derivatives have scaled error below 2.0×10^{-48}; the sampled check does not replace the formal proof.

The module `AmplitudeChart` assembles the actual Fréchet differential of the endpoint in the unwrapped coordinates (a, b, k) of Appendix B. Its endpoint agrees with the concrete trajectory above. The source map to (t, φ, k) has nonzero determinant, and positive time is equivalent to $a < b$. Rotating the planar derivative rows and applying a checked polynomial identity proves the signed amplitude-chart determinant, including either rotation sign and all quarter-period arguments. The resulting quotient of determinants is also proved. Seventeen new axiom audits use only the standard logical axioms. Independent 50-digit differentiation checks 48 signed cases, including 432 matrix entries, with maximum scaled error below 3.5×10^{-48}; this remains sampled corroboration.

The module `RectifiedEndpoint` constructs the explicit inverse source chart and proves both inverse identities. An explicit inverse of the source differential and the inverse function theorem give its joint strict derivative, without an extra inverse-regularity assumption. Composition then proves the actual (t, φ, k) endpoint differential and its compact determinant, and identifies the map with the concrete trajectory formulas. Fourteen new axiom audits use only the standard logical axioms.

The module `Addition` derives the real Jacobi addition formulas from the ODE and two-sided uniqueness. Its rational denominator is at least $1 - k^2 > 0$. The rational triple satisfies both first integrals, unit bounds, the ODE and the correct initial values; no addition identity is assumed. Differentiation and a value at zero then give the epsilon addition formula and its midpoint increment. The module `Midpoint` checks the polynomial substitution $\mathcal{B} = -4J_2/\Delta$ and identifies this J_2 with the counting library's definition. Thus `rectified_det_J2` proves (4) for the actual endpoint differential in (t, φ, k) coordinates; the corresponding zero-set equivalence is also formal. Twenty new axiom audits use only standard logical axioms. These are formal reproductions of classical identities, with no new special-function novelty claim.

The module `CovectorChart` proves that the initial-covector coordinates (t, γ_0, w_0) form a genuine local chart: its strict differential has determinant $-4/k^3$, and the inverse function theorem provides a local inverse. The normalized source and the endpoint are embedded using their actual circle coordinates. Both embeddings have injective differentials, so the formal theorem `stationaryVariation_iff_J2` equates $J_2 = 0$ with a nonzero variation of time and normalized initial covector whose endpoint variation vanishes. This predicate is defined using the two embedded differentials, not using J_2 or a determinant. The unique first scalar root is also transferred to a unique positive physical time with this property. Twenty-seven new axiom audits use only standard logical axioms.

The modules `HamiltonianFlow` and `RadialTime` verify all six published Hamiltonian equations in a real heading lift, their uniqueness on compact time intervals, and radial-time scaling. The source map to the full initial covector has determinant $-t^2/k^3$ and a local inverse for $t \neq 0$. The theorem `unitTime_endpoint` identifies the explicit endpoint with every solution on $[0, 1]$ having the scaled initial covector. Thus the coordinate ODE identification and radial-time normalization are formal, with twenty-three new axiom audits using only standard logical axioms.

The geometric derivation of this coordinate ODE from the normal Hamiltonian, and the equivalence of exponential-map degeneracy with the second-variation definition of conjugacy, remain imported classical results [7, pp. 383–384], [10, §2.1]. Appendix C checks the variational hypotheses analytically and derives the coordinate equations in canonical variables. The adjoint zero-response criterion for the rotating controls is now formalized, as is the annihilator of the augmented linear map under the normal factorization. The Hilbert-space identification and second-variation theorem remain analytic. Appendix B details the local source charts and embedded differential criterion.

The formal development also proves uniqueness of k_0, the quartic coefficient at the

coalescence and the signed fixed-cell splitting (20), with a fifth-order error bound. The module `Splitting` proves existence and local uniqueness for the concrete determinant and the signed two-sided limit in modulus units. In Section 5, the exact period polynomial for the rectified endpoint determinant and the profile identity are formalized. The analytic tangency classification, simplicity of p_n^α, continuity and extrema of p_*, and geometric fold recognition retain steps outside Lean. The module `LargeIndex` proves the ordered-root law, its joint compact uniformity and the critical quadratic rate. The module `EndpointExpansion` verifies all three indexed endpoint expansions in (25) with one compact-uniform remainder bound.

B Endpoint coordinates and the signed determinant

This appendix reconstructs the classical formula (4) in a regular source chart. It is a reproducibility check of [7, §3.3] and [10, eq. (2.10)], not a new determinant formula. Throughout, $0 < k < 1$, $t > 0$, $\psi \in \mathbb{R}$ and $\sigma = s_2 \in \{-1, 1\}$. Let $F(a, k)$ and $G(a, k)$ be the oriented real first- and second-kind integrals, and set

$$a = \operatorname{am}(\psi, k), \qquad b = \operatorname{am}(\psi + t/k, k), \qquad s_a = \sin a,\ c_a = \cos a,\ d_a = \sqrt{1 - k^2 s_a^2},$$

with analogous notation at b. The amplitudes are unwrapped. Define

$$V = G(b, k) - G(a, k), \quad W = F(b, k) - F(a, k) - V, \quad Q = k(c_a - c_b),$$

$$A = \arcsin(k s_a), \qquad B = \arcsin(k s_b).$$

Here the arcsines are principal: their arguments have absolute value strictly below one. Thus A, B are globally smooth real functions and $\cos A = d_a$, $\sin A = k s_a$. The endpoint is

$$x = \sigma(Q \cos A + W \sin A), \qquad y = \sigma(Q \sin A - W \cos A), \qquad \theta = A - B \pmod{2\pi}. \tag{31}$$

The displayed real lift of θ avoids differentiation of a wrapped angle. Direct time differentiation gives the three horizontal equations in Section 2, with $\gamma = 2\sigma \operatorname{am}(\psi + t/k, k)$ and $w = 2\sigma \operatorname{dn}(\psi + t/k, k)/k$. These satisfy $\dot\gamma = w$, $\dot w = -\sin\gamma$ and $w^2/2 - \cos\gamma = 2/k^2 - 1 > 1$. At $t = 0$ the endpoint is the identity. Uniqueness of this smooth ODE identifies (31) with the rotating normal exponential map.

Regular charts and orientation. The initial covector is $(\gamma_0, w_0) = (2\sigma a, 2\sigma d_a/k)$. At fixed a, $\partial_k(2\sigma d_a/k) = -2\sigma/(k^2 d_a)$; $\partial_\psi a = d_a > 0$. Hence, for either rotation sign,

$$\det \frac{\partial(\gamma_0, w_0)}{\partial(\psi, k)} = -\frac{4}{k^2}, \qquad \det \frac{\partial(a, b, k)}{\partial(\psi, k, t)} = -\frac{d_a d_b}{k}, \qquad \det \frac{\partial(\psi, k, t)}{\partial(t, \varphi, k)} = \frac{1}{k}.$$

The phase is understood locally on its circle; these determinants never vanish. Changing σ negates both planar output rows, preserving the endpoint determinant. Thus neither reflection nor a quarter-period phase changes the sign convention in (4).

To make the differential criterion independent of angle lifts, let

$$C_\sigma(t, \varphi, k) = \left(t, 2\sigma \operatorname{am}(\varphi/k, k), \frac{2\sigma \operatorname{dn}(\varphi/k, k)}{k}\right).$$

Its strict differential satisfies $\det DC_\sigma = -4/k^3 \neq 0$. Here γ_0 has period 4π, whereas the endpoint heading has period 2π [7, pp. 383–384]. Use the embeddings

$$I(t, \gamma, w) = (t, \sin(\gamma/2), -\cos(\gamma/2), w/2), \qquad P(x, y, \theta) = (x, y, \cos\theta, \sin\theta).$$

The last three coordinates of I are (h_1, h_2, h_3); hence $h_1^2 + h_2^2 = 1$ and the Hamiltonian energy is $1/2$. The chart also satisfies $w_0^2/2 - \cos\gamma_0 = 2/k^2 - 1 > 1$. Both DI and DP are injective, by $\sin^2 + \cos^2 = 1$. Writing $\widehat{S} = I \circ C_\sigma$ and $\widehat{Q} = P \circ \mathrm{Exp}_\sigma$ in the original elliptic source coordinates, it follows that

$$\exists v \ (D\widehat{S}\, v \neq 0 \text{ and } D\widehat{Q}\, v = 0) \quad \Longleftrightarrow \quad J_2(\tau, p) = 0.$$

The module `CovectorChart` proves these statements for either sign and every real phase, without choosing a global angle chart. It also transfers the first-root uniqueness theorem to physical time $t \in (0, 2kp_1]$. This verifies the normalized endpoint differential criterion. Its interpretation as variational conjugacy uses the classical theorem recalled in [10, §2.1], rather than a Lean formalization of second variations.

From travel time to a full initial covector. Write $\mathcal{H} = (h_1^2 + h_2^2)/2$ for the normal Hamiltonian, distinct from the pendulum energy $H = w^2/2 - \cos\gamma$. In the published convention its equations are

$$\dot{x} = h_1 \cos\theta, \quad \dot{y} = h_1 \sin\theta, \quad \dot{\theta} = h_2, \qquad \dot{h}_1 = -h_2 h_3, \quad \dot{h}_2 = h_1 h_3, \quad \dot{h}_3 = h_1 h_2$$

[7, eqs. (2.5)–(2.6)]. The explicit trajectory together with $(h_1, h_2, h_3) = (\sigma\,\mathrm{sn}(\psi + s/k), -\mathrm{cn}(\psi + s/k), \sigma\,\mathrm{dn}(\psi + s/k)/k)$ solves all six equations. Their vector field is smooth; on a compact interval the images of any two solutions lie in a common compact ball, where the field is Lipschitz. Gronwall's inequality then gives uniqueness for equal initial data. The Lean theorem `hamiltonian_unique_on` needs the ODE only on the comparison interval and continuity at its endpoints.

For a solution $(q(s), h(s))$, direct substitution shows that $(q(ts), th(ts))$ is a solution with initial covector $th(0)$. Consequently the endpoint at travel time t of the normalized solution is the endpoint at time one of the solution with full initial covector

$$\Lambda(t, \gamma, w) = \big(t\sin(\gamma/2), -t\cos(\gamma/2), tw/2\big).$$

Its differential satisfies

$$\det D\Lambda = \frac{t^2}{4}, \qquad \mathcal{H}(\Lambda) = \frac{t^2}{2}, \qquad \det D(\Lambda \circ C_\sigma) = -\frac{t^2}{k^3}.$$

Thus for $t > 0$ this is a regular local change of source coordinates. Time zero is excluded: the radial differential is singular there. The inverse function theorem supplies an actual local inverse; no inverse-regularity hypothesis is added. The kernel criterion above is unchanged if $D\widehat{S}\, v \neq 0$ is replaced by $D(\Lambda \circ C_\sigma)\, v \neq 0$. Together with uniqueness and the injective heading embedding, this justifies passage to the fixed-time full-covector exponential map. These coordinate statements reproduce classical Hamiltonian homogeneity; they are not a new geometric theorem or a formal proof of the second-variation criterion.

Parameter derivatives and algebra. For a fixed $k \in (0, 1)$ choose $r = (k + 1)/2$ and $\delta = \sqrt{1 - r^2} > 0$. At every real u and $0 < q < r$,

$$\sqrt{1 - q^2 \sin^2 u} \geq \delta, \qquad \left|\partial_q \sqrt{1 - q^2 \sin^2 u}\right| \leq \delta^{-1}, \qquad \left|\partial_q \frac{1}{\sqrt{1 - q^2 \sin^2 u}}\right| \leq \delta^{-3}.$$

These constant bounds are integrable on each finite amplitude interval, justifying differentiation under the oriented integral locally in k. The resulting partial derivatives are jointly

continuous in (k, a); thus they give the full differential, not only separate derivatives. With $S(a) = s_a c_a / d_a$, the formulas are

$$F_k = \frac{G}{k(1-k^2)} - \frac{F}{k} - \frac{kS(a)}{1-k^2}, \qquad G_k = \frac{G-F}{k}.$$

These classical identities [8, eqs. (19.4.5)–(19.4.6)] also follow by differentiation in a and their value zero at $a = 0$; they therefore hold for negative and multi-period amplitudes. In the independent coordinates (a, b, k) they give

$$W_a = -\frac{k^2 s_a^2}{d_a}, \qquad W_b = \frac{k^2 s_b^2}{d_b}, \qquad W_k = \frac{k}{1-k^2}\left(V - \frac{s_b c_b}{d_b} + \frac{s_a c_a}{d_a}\right).$$

It suffices to compute for $\sigma = 1$. For each source coordinate i, rotate the planar derivative rows by $-A$. They become $Q_i + WA_i$ and $-W_i + QA_i$; the third row is $A_i - B_i$. This row rotation has determinant one and retains the terms from differentiating A. Expanding this matrix and applying the two source-coordinate factors above gives

$$\det \frac{\partial(x, y, \theta)}{\partial(t, \varphi, k)} = \frac{k}{1-k^2}\,\mathcal{B},$$

$$\begin{aligned}\mathcal{B} = {} & (VW + d_a^2 + d_b^2 - 2k^2)c_a c_b + (V - W)(c_a s_b d_b - c_b s_a d_a) \\ & + 2 s_a s_b d_a d_b - 2(1-k^2).\end{aligned}$$

More explicitly, for the source map $\mathcal{S}(a, b, k) = (k(F(b,k) - F(a,k)), kF(a,k), k)$ and the endpoint map $\mathcal{E}_\sigma$ in (31),

$$\det D\mathcal{S} = -\frac{k^2}{d_a d_b} \neq 0, \qquad \det D\mathcal{E}_\sigma = -\frac{k^3 \mathcal{B}}{(1-k^2) d_a d_b} \quad (\sigma^2 = 1).$$

The module `AmplitudeChart` proves both actual differential formulas and these determinants. The inverse source chart is

$$\mathcal{S}^{-1}(t, \varphi, k) = \big(\mathrm{am}(\varphi/k, k), \mathrm{am}((\varphi + t)/k, k), k\big).$$

Its differential sends $(\delta t, \delta\varphi, \delta k)$ to $(\delta a, \delta b, \delta k)$, where

$$\begin{aligned}\delta a &= \frac{d_a}{k}\big(\delta\varphi - (F(a,k) + kF_k(a,k))\delta k\big), \\ \delta b &= \frac{d_b}{k}\big(\delta t + \delta\varphi - (F(b,k) + kF_k(b,k))\delta k\big).\end{aligned}$$

These formulas follow by inverting $D\mathcal{S}$; the inverse function theorem justifies differentiating the inverse map. The module `RectifiedEndpoint` proves both inverse identities, this derivative, and its composition with the endpoint differential. Taking determinants therefore proves the preceding (t, φ, k) formula, including its sign. The modules `Addition` and `Midpoint` complete the formal midpoint reduction below.

Put $p = t/(2k)$, $\tau = \psi + p$ and $\Delta = 1 - k^2 \operatorname{sn}^2 p \operatorname{sn}^2 \tau$. The Jacobi addition formulas [8, §22.8] express $s_a, c_a, d_a, s_b, c_b, d_b$ in the midpoint variables with denominator Δ; the epsilon addition formula [8, eq. (22.16.27)] gives

$$V = 2\mathcal{E}(p) - \frac{2k^2 \operatorname{sn}^2\tau \operatorname{sn} p \operatorname{cn} p \operatorname{dn} p}{\Delta}, \qquad W = 2p - V.$$

Substitution yields $\mathcal{B} = -4J_2/\Delta$, proving (4) with its stated orientation. In Lean, six exact polynomial identities establish the rational addition ODE and first integrals and the

epsilon derivative; a seventh checks this substitution. The coefficients supplied by symbolic reduction are checked by the Lean kernel, rather than trusted as symbolic-software output. The exact checker `research/e145_endpoint_algebra.py` expands the derivative matrix and reduces this identity using only the sine/cosine and d^2 relations. All canceled factors are among k, $1-k^2$, d_a, d_b and Δ; they are nonzero throughout the stated domain. No division by $\operatorname{sn} p$, $\operatorname{cn} p$ or $\operatorname{sn} \tau$ is used. The sign and zero-set equivalence therefore include the critical coalescence and bracket endpoints.

As a separate check, direct 50-digit endpoint differentiation at 32 signed samples, including negative phases and quarter-period arguments, agrees with the predicted determinant in the column order (ψ, k, t): $-4k^2 J_2/((1-k^2)\Delta)$. The maximum discrepancy divided by one plus the absolute prediction is below 1.2×10^{-49} (`research/e145_signed_endpoint_check.py`). This check compares signed values; it does not accept a choice of sign. It corroborates the exact calculation rather than certifying a sampled domain.

A further independent check differentiates the original endpoint directly in (t, φ, k) and compares it with the signed J_2 formula at 48 cases, including negative initial phases and quarter-period arguments. At 50-digit precision the maximum scaled discrepancy is below 1.5×10^{-49} (`research/e149_determinant_check.py`). A separate 60-digit check of the three Jacobi additions, epsilon addition and midpoint increment makes 200 comparisons over 40 argument pairs, with maximum absolute discrepancy below 1.9×10^{-60} (`research/e149_addition_check.py`). These finite checks corroborate the formal identities; they do not prove geometric conjugacy or classify singularities of the endpoint map.

The source-coordinate determinant and the Gram determinant of $D\widehat{S}$ were also checked independently at 50 digits in 48 signed cases, with scaled discrepancy below 9.9×10^{-48} (`research/e150_covector_check.py`). At six selected Maxwell-phase roots, direct 60-digit differentiation gives a nonzero source variation with normalized endpoint residual below 4.0×10^{-62} (`research/e150_variation_check.py`). These selected checks do not enumerate all roots or prove the second-variation criterion.

An independent radial-time check differentiates Λ at 50 digits in 48 cases, with scaled determinant discrepancy below 2.4×10^{-51}. Separate direct integration of the six Hamiltonian equations agrees with radial-time scaling in three cases to 8.0×10^{-14} and with the elliptic endpoint and covector in eight signed cases to 3.7×10^{-13} (`research/e151_radial_flow_check.py`). These are sampled floating-point checks, separate from the formal proof.

C Applicability of the variational criterion

We spell out the hypotheses behind the passage from a Jacobian zero to variational conjugacy. Use the fixed-time energy functional

$$\mathcal{J}_T(u) = \frac{1}{2}\int_0^T (u_1^2 + u_2^2)\, ds, \qquad u \in L^2([0,T], \mathbb{R}^2).$$

For length $L(u)$, Cauchy–Schwarz gives $\mathcal{J}_T(u) \geq L(u)^2/(2T)$, with equality at constant speed. The normal trajectories used here have unit speed. The energy formulation provides the smooth variational setting; the norm integrand in the length functional is not used to assert the strengthened Legendre condition at zero control. The extremals and their controls are smooth and bounded on compact intervals, so they also meet the admissibility convention of [10, §2.1].

Legendre condition and maximization (H1–H2). The control Hamiltonian and its maximum are

$$\mathcal{H}_u = h_1 u_1 + h_2 u_2 - \tfrac{1}{2}(u_1^2 + u_2^2) = \mathcal{H} - \tfrac{1}{2}\big((u_1 - h_1)^2 + (u_2 - h_2)^2\big).$$

Thus $\partial_u^2 \mathcal{H}_u = -I_2$ and the unique maximizer on $U = \mathbb{R}^2$ is $(u_1, u_2) = (h_1, h_2)$. For clarity, in canonical cotangent coordinates (p_x, p_y, p_θ),

$$h_1 = p_x \cos\theta + p_y \sin\theta, \quad h_2 = p_\theta, \quad h_3 = p_x \sin\theta - p_y \cos\theta.$$

Hamilton's equations for $\mathcal{H}$ give $\dot{p}_x = \dot{p}_y = 0$, $\dot{p}_\theta = h_1 h_3$; differentiation gives exactly the six coordinate equations in Appendix B.

Normal multiplier and corank (H3). Let $E_T(u) = q_u(T)$ be the endpoint map on controls. An abnormal lift would annihilate the horizontal fields, so its momentum components ℓ_1, ℓ_2 vanish identically. Its adjoint equations imply $0 = \dot{\ell}_1 = -u_2 \ell_3$ and $0 = \dot{\ell}_2 = u_1 \ell_3$. Since $u_1^2 + u_2^2 = 1$ along the trajectories under consideration, $\ell_3 = 0$ also. The three fields $X_1 = (\cos\theta, \sin\theta, 0)$, $X_2 = (0, 0, 1)$ and $[X_1, X_2] = (\sin\theta, -\cos\theta, 0)$ form a basis, so the lift would be zero, a contradiction. This applies on every nontrivial subinterval; there are no abnormal segments. It is also the contact case of [1, Proposition 4.38, p. 116].

Consequently DE_T is surjective. The normal multiplier satisfies $D\mathcal{J}_T = \lambda_T DE_T$, and is unique: the difference of two such multipliers would annihilate DE_T. Hence the augmented map $u \mapsto (E_T(u), \mathcal{J}_T(u))$ has differential of corank one (cf. the endpoint-and-cost map in [1, p. 350]). This makes the endpoint-and-cost interpretation of H3 explicit; the position endpoint map itself is regular. Neither statement prescribes the corank of the finite-dimensional exponential map at a conjugate time.

Completeness (H4). For arbitrary initial covectors, $\mathcal{H}$ is conserved, as follows from $h_1 \dot{h}_1 + h_2 \dot{h}_2 = 0$. Writing $C = \mathcal{H}(0) \geq 0$, one has

$$|h_1|, |h_2| \leq \sqrt{2C}, \qquad |\dot{h}_3| = |h_1 h_2| \leq C, \qquad |\dot{x}|, |\dot{y}|, |\dot{\theta}| \leq \sqrt{2C}.$$

Thus all six lifted coordinates remain bounded on each finite time interval, including when $C = 0$. The vector field is smooth on $\mathbb{R}^6$, so the continuation theorem for ordinary differential equations excludes a finite maximal forward time. Projection of the real heading lift gives completeness on $T^* \mathrm{SE}(2)$.

These checks justify use of the classical criterion in [10, §2.1, pp. 1021–1022]. Equivalently, [1, Proposition 8.54, p. 239] identifies exponential-map degeneracy with degeneracy of the constrained energy Hessian along normal trajectories without abnormal segments. Together with the regular radial-time chart, this applies to the normalized J_2 criterion for every $t > 0$, including the exceptional phase and modulus. The criterion itself is an imported theorem.

As an independent check of the distinction between the two control maps, `research/e152_variational_check.py` integrates their linearized Gramians in 24 signed cases, including critical-coalescence times. The position Gramian has positive least eigenvalue in every sample; the augmented Gramian has one numerically zero eigenvalue and three positive ones. Its normalized residual against the normal multiplier is below 9.6×10^{-13}. These floating-point samples corroborate the analytic corank argument and do not establish it for all controls.

AI assistance

This paper was prepared with the assistance of Claude (Anthropic), a large language model used through the Claude Code agent in September 2026. The model drafted and restructured the text and the proofs, wrote the figure and verification code, ran the checks of Section 6 and wrote the Lean formalization; the identity for $\alpha_1/\operatorname{dn} p$ in Lemma 3.1, the large-index law, the Floquet form and the separatrix limits were first found with its help; the text was further revised with OpenAI Codex, which also assisted the October 2026 tangency argument and its Lean implementation, and the concrete inverse-integral construction of the Jacobi functions in Lean, the endpoint trajectory formalization and signed determinant audit, the joint elliptic-integral derivative formalization, and the amplitude-chart differential, determinant and inverse-coordinate proofs. The scope of the formal, symbolic and numerical checks is described above. Responsibility for the final statements and submission remains with the author.

References

[1] Andrei Agrachev, Davide Barilari, and Ugo Boscain. A comprehensive introduction to sub-Riemannian geometry: From hamiltonian viewpoint. Draft of 6 February 2019, 643 pages; cited proposition and page numbers refer to this draft, 2019.

[2] Andrei A. Agrachev and Yuri L. Sachkov. *Control Theory from the Geometric Viewpoint*, volume 87 of *Encyclopaedia of Mathematical Sciences*. Springer, Berlin, 2004.

[3] Davide Barilari and Luca Rizzi. Comparison theorems for conjugate points in sub-Riemannian geometry. *ESAIM: Control, Optimisation and Calculus of Variations*, 22(2):439–472, 2016.

[4] Igor Moiseev. The conjugate locus of the rotating geodesics in the sub-Riemannian problem on SE(2). Preprint in preparation; source `manuscripts/first_caustic_se2.tex` in the repository `https://github.com/moiseevigor/se2-conjugate-locus`, 2026.

[5] Igor Moiseev. elliptic-functions: elliptic integrals and functions for NumPy, PyTorch and JAX, version 4.1.0. `https://github.com/moiseevigor/elliptic`, 2026.

[6] Igor Moiseev. Scalar inversion and geodesic counts by winding on SE(2). Preprint in preparation; source `manuscripts/inversion_counts_se2.tex` in the repository `https://github.com/moiseevigor/se2-conjugate-locus`, 2026.

[7] Igor Moiseev and Yuri L. Sachkov. Maxwell strata in sub-Riemannian problem on the group of motions of a plane. *ESAIM: Control, Optimisation and Calculus of Variations*, 16(2):380–399, 2010.

[8] NIST Digital Library of Mathematical Functions. NIST digital library of mathematical functions, chapters 19 (elliptic integrals) and 22 (jacobian elliptic functions). `https://dlmf.nist.gov/`. Release 1.2.7, accessed 1 September 2026.

[9] Yuri L. Sachkov. Maxwell strata in the Euler elastic problem. *Journal of Dynamical and Control Systems*, 14(2):169–234, 2008.

[10] Yuri L. Sachkov. Conjugate and cut time in the sub-Riemannian problem on the group of motions of a plane. *ESAIM: Control, Optimisation and Calculus of Variations*, 16(4):1018–1039, 2010.

[11] Yuri L. Sachkov. Cut locus and optimal synthesis in the sub-Riemannian problem on the group of motions of a plane. *ESAIM: Control, Optimisation and Calculus of Variations*, 17(2):293–321, 2011.

[12] Yuri L. Sachkov. Left-invariant optimal control problems on Lie groups that are integrable by elliptic functions. *Russian Mathematical Surveys*, 78(1):65–163, 2023.